Transcriptomic Regulations Underlying Pair-Bond Formation and Maintenance in the Socially Monogamous Male and Female Prairie Vole

Supplement 1

Supplementary Methods

Animals

Sexually-naive male and female prairie voles (*Microtus ochrogaster*) from a laboratory breeding colony were weaned at 21 days of age and housed in same-sex sibling pairs in plastic cages (12 × 28 × 16 cm) with water and food provided ad libitum. All cages were maintained under a 14:10 h light-dark cycle, and the temperature was approximately 20 °C. All animals were randomly assigned into experimental groups when they reached 70–90 days of age. Experimental procedures were approved by the Institutional Animal Care and Use Committee at Florida State University.

Cohabitation and resident-intruder test

In prairie voles, the formation of a social bond can be observed following a prolonged cohabitation with an opposite-sex conspecific. While 24 hrs of cohabitation with a partner are sufficient to reliably induce the formation of partner preference in prairie voles, indicator of the initiation of the pair-bond, prolonged cohabitation for at least two weeks are generally considered in the maintenance phase of the pair-bond (1,3,5,7). Accordingly, differences in key factors (oxytocin receptor, OTR, and the vasopressin V1a receptor, V1aR) have been reported at these timepoints (5,9,11), thereby providing evidence for differences in gene expression in the Nucleus Accumbens (NAc) following 24 hrs, and at least two weeks of cohabitation with a partner. Intact male and female prairie voles were thus paired and cohabitated with an aged-matched opposite-

sex partner for 3 weeks (“3W” group, later phase of the pair-bonding process) or 24 hours (“24H” group, early phase of the pair-bonding process), or a same-sex littermate for 3 weeks (Sexually Naive, “SN” group). Notably, the stimulus animals used for opposite-sex cohabitation were ovariectomized or vasectomized as previously described (7) in order to prevent any uncontrolled effects due to pregnancy. Furthermore, stimulus females used for the males in the 24H group were estrogen-primed (2 µg per day, *i.p.* for 3 days)(9) to ensure the development of a pair-bond.

Following 3 weeks or 24 hrs of cohabitation, selective aggression behavior was assessed using a resident-intruder test (RIT) as previously described (13). Briefly, the stimulus partner was removed from the home cage, and a same-sex stranger conspecific was introduced to the test subject and left to freely interact for 10 minutes. The session was video-recorded and the following behaviors of the resident (test subject) were scored *a posteriori* by a trained experimenter blind to the treatment groups using JWatcher (v1.0)(15): aggressive behaviors (attacks, bites, chases, offensive upright postures), anogenital sniffing, nose-to-nose sniffing, defensive behaviors, side-to-side contact (huddling), as well as non-social cage exploration. All other behaviors were scored as “Other”. Notably, all procedures were scheduled so that all biological groups (SN, 24H, and 3W) would be represented in each day of testing and sample collection within each cohort, to limit interference of external factors such as day of experimental testing or age with data interpretation. As a result, voles from all biological groups were age-matched at the time of testing and sample collection.

RNA extraction, library preparation, and sequencing

Immediately after RIT, subjects were killed by rapid decapitation, their brain dissected out, snap-frozen, and stored at -80C until further processing. Total RNA was then extracted from nucleus accumbens (NAc) tissue punches using the TRI-Reagent protocol according to the manufacturer’s instructions (Molecular Research Center, Cincinnati, OH, USA), followed by DNAse I treatment to remove any eventual DNA contamination and clean-up (RNA Clean &

Concentrator, Zymo Research, Irvine, CA, USA). RNA quality and integrity were then verified electrophoretically on an RNA Nano 6000 Bioanalyzer chip (Agilent, Santa Clara, CA, USA), whereas RNA concentration was measured spectrophotometrically (Nanodrop, Thermo Fisher Scientific, Waltham, MA, USA).

RNA-seq libraries were prepared using the NEBNext Ultra RNA Library Prep Kit for Illumina with poly(A) mRNA purification from 300 ng of total RNA based on magnetic beads, cDNA synthesis using random hexamers, and final amplification using barcoded primers following the manufacturer's protocol (#E7530, New England Biolabs, Ipswich, MA, USA). To determine the lower limit of detection and verify the linearity of quantification during the statistical analysis of the sequencing data, synthetic RNA Spike-Ins (#4456739, ERCC ExFold RNA Spike-In Mixes, Life Technologies, Carlsbad, CA, USA) were added to each sample prior to poly(A) mRNA purification following the recommended dilutions (6 µL of a 1:1000 dilution). Of note, Mix 1 and Mix 2 of the ERCC ExFold RNA Spike-Ins were equally distributed among samples in an exclusive manner. The resulting barcoded and unstranded libraries were quantified using a KAPA qPCR library quantification kit (KAPA Biosystems, Boston, MA, USA) with three serial dilutions ran in duplicate on a CFX384 real-time PCR instrument (Bio-Rad). Finally, the absence of adapter or primer contamination was verified on a Bioanalyzer using a DNA High Sensitivity chip (Agilent Technologies, Santa Clara, CA, USA). A total of 46 libraries were thus generated: 16 voles from the SN group (6 males, 10 females), 16 voles from the 24H group (6 males, 10 females), and 11 for the 3W group (5 males, 6 females). All libraries were then pooled and sequenced (2x50bp, NovaSeq 6000, S2 lane) at the Translational Sciences Laboratory at Florida State University. This design generated a total of 1,993.47 M paired-end raw reads (passing filter, >Q30, and demultiplexed), with a median number of reads per biological sample of 44.40 M. The data discussed in this publication have been deposited in NCBI's Gene Expression Omnibus (17) and are accessible through GEO Series accession number GSE150080.

Data processing

Raw reads were first processed for quality filtering and adapter trimming with fastp (v0.14.1)(19), followed by verification of good quality using FastQC (v0.11.7)(21) before pseudo-alignment and quantification using Salmon (v0.12)(23). Notably, quantification was done using Ensembl annotations (release 93) of the prairie vole genome (MicOch1.0, GCA_000317375.1) to which the *Avpr1a* gene sequence (AF069304) was manually added. Quantifications were thus summarized at the gene level (25) and processed for differential expression analysis using DESeq2 (v1.20.0)(27,29) and a false discovery rate of 10%. Prior to proceeding to the differential expression analysis, reads mapped quantified to ERCC spikes-ins were processed through both the DESeq2 analysis pipeline to assess the lower limit of detection, from which the minimum number of reads for an accurate measure of gene expression was calculated. Genes that did not satisfy this minimum number of uniquely mapped reads were discarded from the dataset before statistical analysis.

Functional analysis

Gene-Sets Enrichment Analyses (GSEA, v3.0)(31) were performed as previously described (21) using gene-sets comprising pathway annotations for mouse curated from public databases (http://download.baderlab.org, September_01_2018 release), and the resulting enriched pathways were visualized using the Cytoscape (v3.6.0)(22) enrichment map plugin (35), following the author's recommendations (37). Notably, gene annotations in RNAseq matrices were enhanced with known gene orthologues from the mouse genome fetched from Biomart (Ensembl release 93)(38). To do so, prairie vole Ensembl gene ids without gene symbol were attributed their corresponding gene symbol from mouse orthologs with a "one-to-one" relationship (this resulted in 1,000 more genes annotated with a gene symbol). This procedure was then repeated for those remaining without a gene symbol by using the mouse orthologs with a "one-to-many" relationship; in such case all mouse orthologs for a given prairie vole gene were sorted

(in order) based on confidence of homology (high or low), mouse gene-order conservation score, followed by percentage of identity with the query gene, and the best (top) hit was kept. This resulted in an additional 1,176 genes annotated for a total of 17,278 genes annotated with gene symbol.

The regulation of genes by estrogens and progestins was analyzed by comparing our list of DEG with those that were previously identified as being regulated by estrogens, progestins, or androgens in the Comparative Toxicogenomics Database (39) as of November 8th, 2018. Differentially expressed genes with a previously reported regulation by either estrogens, progestins, or androgens were extracted, and the enrichment of either group in the dataset was tested using Fisher's exact test in R (40). Similarly, the enrichment in autism spectrum disorders-related genes was performed by leveraging the list of genes of interest curated in the SFARI Gene database in their March 4th, 2020 release (41,42) to extract genes with a "gene score" greater than 0, or "syndromic" status of 1; the enrichment in such genes was then tested using Fisher's exact test in R. Furthermore, the enrichment of related gene ontologies and Kyoto Encyclopedia of Genes and Genomes (KEGG) pathways was tested using the Bioconductor package clusterProfiler (v3.10.1) (43).

Differential transcript usage analyses

The analysis of differential transcript usage (DTU) was performed following a previously described pipeline (44). Briefly, following estimation of transcripts abundance by Salmon (v0.12)(23), a DTU was conducted using the Bioconductor package DRIMSeq (v1.8.0) (45) after filtering the dataset using the same criteria as in the published pipeline (44). The StageR package (v1.2.22) (46) was used to first identify which genes show evidence of DTU, followed by identification of the responsible transcript(s) within each gene. The procedure was performed using post-hoc filtering on the standard deviation in proportion, with an overall false discovery rate of 0.1 (44).

Gene network analyses

A weighted gene co-expression network analysis was conducted using the R package WGCNA (v1.68) (47–49) following the authors' recommendations. Notably, as the extent of sex differences at each cohabitation timepoint was substantial, signed co-expression networks were first constructed within each sex using biweight mid-correlation. Following the authors' instructions, consensus clusters of gene expression (modules) were then extracted, and behavioral traits (behavioral measurements during the RIT) were then related to consensus modules eigengenes within each sex. Following a principal component analysis of the behaviors scored during the RIT, we computed a Resident-Intruder score (R.I.) as RI = Aggression - Anogenital sniffing - nose-to-nose sniffing (for durations and frequencies, separately) and included it as an additional behavioral trait. As a result, while each gene was assigned to a single module, we obtained two sets of consensus module eigengenes as a given module might have a particular expression profile in females, and a different pattern in males. While 26 consensus modules were thus identified, the modules most related to our behavioral data (and significant with $p < 0.05$) were extracted by sorting the matrices of biweight mid-correlation according to the following criteria (in order): aggression frequency, aggression duration, nose-to-nose frequency, nose-to-nose duration, as well as the binary traits related to group membership 3W_vs_All, 3W_vs_SN, and 3W_vs_24H—each considering their *p*-value first, followed by the correlation value. Finally, we assessed within each module the relation between each gene's significance for each behavioral trait and its module membership to verify the presence of a strong link between the two variables, following the authors' instructions (47–49). This revealed that the correlations of the genes included in the salmon and magenta modules in males were not supported by a strong link between gene significance and module membership and were thus excluded from the list of modules of interest used for gene networks analyses.

To further investigate gene-gene interaction networks, ARACNe-AP (Algorithm for the Reconstruction of Accurate Cellular Networks with Adaptive Partitioning)(50) was first run on all

modules and groups of modules of interest identified by WGCNA to highlight significant interactions between genes and remove indirect interactions. ARACNe-AP was run using 100 reproducible bootstraps that were then reconsolidated. The expression files required by ARACNe-AP were prepared using the rlog-transformed read counts from DESeq2, together with a list of transcription factors annotated in prairie voles (1,345 transcription factors total) using annotation of mouse orthologs from the Transcription Co-Factor database (as of October 2018) (51). A key driver analysis was then conducted from the resulting ARACNe-AP-defined unweighted networks using the Bioconductor package Mergeomics (v1.16) as previously described (52–54), allowing the identification of key driver genes referred to as “hub” genes. The final networks were visualized using Cytoscape.

Analysis of mRNA and mtDNA levels by real-time PCR

Thirty nanograms of total RNA from NAc samples (including the samples used for RNA-seq libraries) were reverse-transcribed using the LunaScript RT SuperMix Kit (New England BioLabs, Ipswich, MA, USA) and analyzed by semi-quantitative real-time PCR as previously described (55), with normalization to hypoxanthine phosphoribosyltransferase 1 (*Hprt1*) gene. For mtDNA copy number estimation, 30 ng of genomic DNA (extracted alongside total RNA using the TRI-reagent protocol) were used and normalization was performed against the nuclear gene glyceraldehyde 3-phosphate dehydrogenase (*Gapdh*). All reactions were performed in triplicate on a CFX384 thermocycler (Bio-Rad), and their specificity was verified by melting curve analysis. All primers used are detailed in Table S7.

Mitochondrial respiration measurements

Adult male and female prairie voles were cohabitated with a same-sex littermate (SN) or opposite-sex partner (24H) for 24 hrs. To verify the establishment of a bond, both members of the pairs were subjected to a RIT and killed immediately after. Their brain was dissected out, and

tissue punches of the NAc were collected and used for measurement of mitochondrial respiration the same day. High-resolution O_2 consumption measurements (56) were conducted at 37°C in buffer Z supplemented with creatine monohydrate (20 mM), using the OROBOROS O2K Oxygraph. The protocol was based on previous studies establishing the optimal conditions for measurements of mitochondrial respiration brain samples (57,58). Samples were incubated in saponin (50 µg/ml) for allowing permeabilization followed by a substrate inhibitor titration protocol. The protocol was as follows: 5mM pyruvate, 2 mM malate and 10 mM glutamate (state 2 respiration), followed by the addition of 4 mM ADP to initiate state 3 respiration supported by complex I substrates. Convergent electron flow through complexes I and II was initiated with the addition of 10 mM succinate followed by 10 µM rotenone to inhibit complex I. To test the integrity of the mitochondrial membrane we added 10 µM cytochrome c. Complex IV–supported respiration was examined using the electron donor *N,N,N′,N′*-tetramethyl-*p*-phenylenediamine (TMPD) at 0.4 mM in the presence of 2 mM ascorbate (to limit auto-oxidation of TMPD) and 5 µM of antimycin A (to prevent reverse electron flow through complex III). The rate of respiration was expressed as pmol/s/mg of protein. All respiration measurements were conducted at 37°C and a working range [O2] of approximately 350 to 200 µM.

In addition, citrate synthase activity assays were performed using a citrate synthase activity assay kit (Sigma-Aldrich, St Louis, MO, USA, CS0720) per the manufacturer's instructions. Briefly, brain sample lysates were generated by glass pestle homogenization by hand in RIPA buffer. Protein concentrations were determined using a Pierce BCA protein assay (Thermo Fisher Scientific, Waltham, MA, USA, cat. #23225). Activity assays were performed in assay buffer containing 100 mM Tris, 1 mM EDTA, 1 mM EGTA, 10 mM DTNB (Sigma-Aldrich, St Louis, MO, USA, cat. #D8130), and 30 mM acetyl CoA at pH 8.35. All samples were measured in duplicate and the average absorbance was used in final calculations of activity. Background absorbance was measured prior to addition of 10 mM oxaloacetate (Sigma-Aldrich, St Louis, MO, USA, cat. # O4126) and final activity rates were corrected for those values.

Statistical analyses

Data were analyzed with the Prism (v8.2.0, GraphPad Software, San Diego, CA, USA) or R (40) softwares by two-way analysis of variance using “Cohabitation” (SN, 24H, 3W) and “Sex” as independent factors, followed by Tukey’s post-hoc test when a main effect was statistically significant at alpha = 0.05.

Supplementary Results

Behavioral characterization throughout the resident-intruder test

To better understand and characterize the complex behavior of selective aggression, we further analyzed the different behaviors scored during the resident-intruder test (RIT) by investigating for each animal the distribution of time spent displaying each behavior either throughout the entire 10 min session, or with 30 sec timebins.

As expected, and in line with the individual analyses of each behaviors (Fig. 1, Fig. S1, Table S1), both male and female prairie voles paired with an opposite-sex partner for either 24 hrs (24H) or 3 weeks (3W) exhibited higher selective aggression behaviors towards the intruder when compared to sexually-naive (SN) controls (Fig. S2A). This increased aggressivity was associated with a reduction in non-aggressive social interactions (*i.e.* anogenital sniffing and nose-to-nose sniffing) as well as in non-social exploratory behaviors to a lesser extent (Fig. S2A). When investigating the evolution of the distribution of time spent in each behavior (Fig. S2B), we can see that all groups exhibited a sharp increase in anogenital and nose-to-nose sniffing during the first minute following the introduction of the unfamiliar intruder, indicating an initial investigation of the intruder by all groups regardless of sex or cohabitation status. Interestingly, however, while SN males and females showed a slow reduction in anogenital and nose-to-nose sniffing thereafter, both males and females cohabitated for 24 hrs or 3 weeks exhibited a sharper decline in anogenital and nose-to-nose sniffing accompanied by the appearance of aggressive behaviors. This therefore suggests that pair-bonded voles differ from SN controls only after the initial investigation and identification of the test subject as an unfamiliar intruder, in line with the selective nature of their aggressive behaviors reflective of nest-guarding behavior.

Contribution of estrogens and progestins to the transcriptomic regulations in the prairie vole NAc underlying pair-bonding

Unlike rats or mice, estrus in female prairie voles is triggered by exposure to male cues that induces a surge in estrogens levels (59–63). Considering the well-known genomic effects of estrogens and their receptors in rodents, together with their known modulation of multiple aspects of social attachment and pair-bonding in prairie voles (1,64–66), we further aimed at estimating the contribution of estrogens, progestins, as well as androgens, to the transcriptomic changes seen in the NAc of male and female prairie voles following cohabitation with an opposite-sex partner. Interestingly, we found a significant enrichment of genes with known regulation by estrogens and progestins in the DE genes in 24H females when compared to SN controls, as well as in sexually-biased genes following 3 weeks of cohabitation (Fig. S9). Notably, the enrichment in the set of differentially expressed genes following 24 hrs of cohabitation in females was higher than in the sexually-biased genes following 3 weeks of cohabitation (Fig. S9), which is consistent with a greater impact related to the initial surge in estrogens.

In the latter, however, it is interesting to note the enrichment of progestins-regulated genes, in line with the increase in serum progesterone levels following 72 hrs but not 24 hrs of cohabitation with mating, delayed when compared to estradiol levels (62). At the functional level, these estrogens- and/or progestins-responsive genes relate to some of the main biological processes and pathways identified in our study: regulation of energy production and RNA translation in the early phase, and regulation of neurotransmission in the later phase of the pair-bonding process (Fig. S10). Further supported by the well-described effects of estrogens and progestins on these processes in the brain (67–69), these data thus highlight estrogen and progesterone amongst the main contributors directing the reprogramming of gene expression in the prairie vole NAc following cohabitation with an opposite-sex partner.

Sex differences in gene expression

At baseline and following 3 weeks of cohabitation with an opposite-sex partner, we observed a high degree of sexually-biased gene expression in the prairie vole NAc (7.87% and 9.60% of all genes detected, respectively; Fig. 2D,F, Table S2). While the extent of sex differences in the prairie vole transcriptome hasn't been reported previously, the mammalian brain does exhibit widespread sex differences in gene expression and RNA splicing (67,68,70–72). In humans, for instance, up to 2.6% of sex bias is observed throughout the brain (70), but substantially varies between brain areas and developmental stages (70,72). In this context, the relatively high degree of sex bias we observed in the prairie vole NAc (7.87 – 9.60%) could thus reflect a specie effect, or a particularly pronounced sexual dimorphism of the NAc.

Accordingly, we observed a widespread enrichment of gene-sets between males and females at baseline (Fig. 5). Gene-sets related to RNA translation, energy production, myelination, and protein folding, were upregulated in males, whereas those related to neurotransmission, intracellular signaling pathways, epigenetic mechanisms, RNA splicing, extracellular matrix, as well as higher order processes such as social behavior, fear response, or learning and memory, were upregulated in females (Fig. 5). In light of the substantial enrichment of gene-sets related to neurotransmission and synaptic plasticity in female prairie voles when compared to sexually-naive males, our observations would thus point towards higher levels of neuronal activity or plasticity in the female NAc when compared to males. Interestingly, such marked sex differences in NAc physiology have been described in rats and mice at baseline, although with a substantial regional dependency as well as interaction with the female estrous cycle (73). For instance, while female rats show higher mEPSC frequency than males in the core region of the NAc, but not in the NAc shell (74,75), the electrophysiological properties of medium spiny neurons (MSN) in the NAc core of female rats vary throughout the estrous cycle (76).

Sex differences in differential transcript usage

In the mammalian brain, alternative splicing events are particularly enriched and represent an important regulatory step in gene expression with widespread sex differences (70,77). Accordingly, our analyses above revealed that genes related to RNA splicing exhibited a substantial sex bias at baseline and a sex-specific response following cohabitation with an opposite-sex partner (Fig. 3, Fig. 4, Fig. 5). We thus aimed to characterize the transcriptomic regulations in the prairie vole NAc related to pair-bonding by conducting a differential transcript usage analysis. Because of its nature, such analysis relies on the quality of the reference genome's annotation and only considers the genes that have more than one transcript identified. In prairie voles, 5,773 genes (25.06% of all genes) have two or more transcripts annotated, and relate substantially to several aspects of neurotransmission including synapse organization and signal transduction (Fig. S11). Although this represents a smaller proportion of genes when compared to the mouse or human annotations (mouse: 34.37%, human: 29.69%, Fig. S11), this supports the high relevance of those annotated genes with the regulations in neuronal plasticity underlined by our gene expression analyses above.

The analysis of the number of genes with at least one differential transcript usage revealed a pattern similar to the analysis of differentially expressed genes (Table S8, Fig. S12). Indeed, the most prominent changes observed following cohabitation occurred at the 24 hrs timepoint in both males and females when compared to SN controls (males: 53 genes, females: 32 genes), or to voles cohabitated for 3 weeks in males (43 genes) and to a lesser extent in females (11 genes). Moreover, the extent of regulations following 24 hrs overtook the otherwise pronounced sex bias at baseline and following 3 weeks of cohabitation (SN: 81 genes, 24H: 11 genes, 3W: 45 genes). Surprisingly, however, a substantial enrichment of mitochondria-related cellular components and KEGG pathways was observed in those sexually-biased genes, as well as in genes affected by cohabitation in males, but not in females (Fig. S12). Despite the current state of transcripts annotation in prairie voles, these data do further support the involvement of

mitochondrial-related processes in the formation and maintenance of a pair-bond in the prairie vole NAc, and suggest a bigger preponderance of transcript-level regulations in males than in females.

Cohabitation with a partner recruits different gene networks in males and females

Upon analyzing and extracting modules of gene co-expression based on their relation with behavioral performance during the RIT—used as an proxy for the evaluation of the pair-bond—we observed two types of modules.

The first, termed common, were found significantly related to at least one main RIT behavior in both males and females, and include saddlebrown, cyan, green, royalblue, plum1, and violet (6 out of 14 modules of interest in males, 6 out of 15 in females, Fig. S5). While the cyan, saddlebrown, and violet modules are positively associated with aggression and the 24H state but negatively associated with the SN or 3W *vs.* 24H states, green and royalblue, on the other hand, are negatively associated with aggression and the 24H state but positively associated with nose-to-nose sniffing and the SN state (Fig. S5). Despite being linked to behavior performances during the RIT in both males and females, the plum1 module shows an interesting sex-specific relation. Indeed, while plum1 is negatively associated with the 24H state but positively with the 3W and 3W *vs.* All states in males, it is positively associated with the 24H state but negatively with the SN state in females (Fig. S5).

The second type of modules, on the other hand, exhibited a significant relation with at least one of the main behaviors during the RIT in one sex only—either males, or females. In males, the yellow, orangered4, orange, and tan modules are positively associated with aggression and the 24H state while being negatively associated with the SN state. The magenta, salmon, and pink modules, on the other hand, are negatively associated with the 24H state. In females, the brown, darkgreen, and blue modules are positively associated with the 24H state but negatively with the SN state, whereas the lightyellow, turquoise, red, and midnightblue are

negatively associated with aggression and the 24H state, but positively with the nose-to-nose behavior and SN state (Fig. S5).

Interestingly, the underlying genes are generally associated with distinct biological processes and pathways between groups of modules, which thereby supports the functional relevance of the resulting clustering. In particular, the genes included in the modules of interest common between males and females associate with multiple aspects of mitochondrial function (cyan-saddlebrown) as well as RNA translation and splicing (cyan-saddlebrown and green-royalblue, Fig. S6), which further supports their involvement in the regulation of a pair-bond suggested by our observations above. In male-specific groups of modules, however, the genes comprising the pink module relate to protein degradation whereas those in the yellow-orangered4-orange-tan group of modules relate directly to neurotransmission. Finally, in female-specific groups of modules, while the greenyellow and yellowgreen modules are associated to epigenetic modifications and myelination processes, respectively, the genes underlying the lightyellow-turquoise-midnightblue group of modules are enriched in terms related to extracellular matrix interaction and downstream signaling pathways (Fig. S6).

Having further identified modules of interest in each sex and their functional associations, we then aimed at exploring the underlying genes involved as well as identifying candidate driver genes through network and key-driver analyses. For each group of modules of interest identified above, we thus leveraged a combination of factors—including their expression data and transcription factor status—to estimate direct relationships and driver gene status based on the extent of a given gene's connections (52,53). We thus obtained networks of predicted gene interactions in all categories of groups of modules of interest—those common between males and females, as well as those specific to either males or females—and highlighted several candidate key driver genes (hub genes)(Fig. S13-17). Interestingly, the superposition of differential gene expression information reveals that the candidate hub genes showing differential expression following cohabitation in female or male groups of modules do so in females or males,

respectively, whereas those in groups of modules common between males and females were found differentially expressed following cohabitation in either sex (Table S9). Altogether, these observations support the presence of distinct networks of gene interaction following cohabitation with an opposite-sex partner in male and female prairie voles.

In this context, it is particularly interesting to find the *Fos* and *Dusp1* genes as 3W-specific genes upregulated in males (Table S6). Indeed, in the NAc, both genes are critical components of the neurobiological mechanisms underlying reward sensitivity, and are thus repeatedly altered in response to drugs of abuse (78). For instance, *Dusp1* and *Fos* mRNA levels are upregulated in the NAc following single injection of cocaine (79) or methamphetamine in rats (80), MDMA in mice (81), as well as following prolonged exposure to alcohol (82) or in a rat model of heroin addiction (83). Notably, *Dusp1* mRNA levels up-regulation following MDMA injection is dependent on D1R but not D2R (81), which is in line with the increase in D1R but not D2R following 2 weeks of cohabitation in prairie voles (5). Alongside *Dusp1* and *Fos*, mRNA levels for the neuropeptide neurotensin (*Nts*) were upregulated in the NAc of males following cohabitation with a female (Table S10). Neurotensin is a critical modulator of dopaminergic neurotransmission in the NAc and throughout the mesolimbic system (84), and has thus been involved in the regulation of a variety of motivated behaviors including response to reward, sociosexual activity, as well as maternal aggression in rodents (85). In particular, stimulation of neurotensin-expressing neurons in the medial preoptic area projecting to the ventral tegmental area promotes social approach and interaction with an opposite-sex conspecific in mice, through increase in dopamine release in striatal areas (86). Altogether, and although causality remains to be established, these observations do highlight multi-level regulations of critical modulators of dopaminergic neurotransmission. Given that, in prairie voles, exposure to the partner stimulate dopamine release in the NAc (7) and that pair-bonded enhances electrically-evoked dopamine release (5), these regulations could thus represent indicators of, or participate to explain, a sustained and

heightened dopaminergic transmission in the NAc of male prairie voles following prolonged cohabitation with an opposite-sex partner.

Alterations in neurotransmission-related genes and gene-sets

Whether at the transcript, gene, gene-set, or gene network level, our analyses highlight widespread alterations in gene expression following pair-bonding that encompass multiple processes required for a sustained regulation of neurotransmission. Indeed, despite sex- and time-specificities, we repeatedly found alterations in gene-sets related to proteins turnover, synapse organization, DNA transcription, or energy production, and many of the candidate driver genes we identified are known regulators of these processes (Supplemental Results, Table S9). It is important to note that the strength of neuronal connectivity between the medial prefrontal cortex and the NAc directly modulates the development of affiliative behaviors leading to partner preference in female prairie voles (87). Moreover, pair-bond formation is accompanied by the development of the neuronal population responding preferentially to the partner over a stranger in the prairie vole NAc (88). It is therefore tempting to hypothesize that the strengthening or development of specific neuronal connections in the prairie vole NAc allows for the establishment and imprinting of the partner's valence that reflects the enduring nature of the pair-bond. In this context, the widespread regulations related to neurotransmission we uncovered could represent the molecular correlates of such process. Supporting this hypothesis, protein degradation, for instance, is commonly linked to reward processing and its impairments. In mice, while morphine increases poly-ubiquitination levels in the NAc, the proteasome inhibitor lactacystin blocks morphine-induced conditioned place preference, behavioral sensitization, as well as heroin self-administration (89,90). Similarly, the E3 ubiquitin ligases Trim3 (up-regulated in males at 24H when compared to SN controls) and SMURF1 (higher in females than males in SN controls) in the NAc mediate cocaine seeking in mice (91,92), whereas phosphorylation of the proteasome subunit Rpt6 regulates behavioral sensitization to cocaine (93). Impairments in synaptic plasticity

also represent core components in the pathogenesis of autism spectrum disorders (ASD) (94), characterized by deficits in social communication, social interactions, as well as in the ability to form social attachments (95). Moreover, extensive genetic and whole-exome studies identified key regulators of synaptic plasticity through DNA transcription, RNA translation, protein degradation, as well as synaptic organization as ASD risk genes (96–99). In this context, it is particularly interesting to find—in the prairie vole NAc—an enrichment of genes associated to the ASD pathology in the sexually-biased genes at baseline and at 3W (Fig. S18, Table S11, Supplemental Results).

Sex-specific alterations of mitochondria

In light of the widespread changes in gene expression related to mitochondrial state and function observed in females as early as following 24 hrs of cohabitation (Fig. 4, Fig. 5), we further aimed at testing whether mitochondrial activity would be altered in the early phase of the pair-bonding process. To do so, male and female prairie voles were cohabitated for 24 hrs with an opposite-sex partner (24H), or a same-sex littermate (SN). Immediately following verification of a pair-bond—estimated by levels of selective aggression exhibited during a RIT session—we proceeded with the measurement of citrate synthase activity as a functional indicator or mitochondrial density (100–102), as well as several components of the electron transport chain by high resolution respirometry (Fig. S7A). We thus found that citrate synthase activity and the complex I to complex II junction showed a similar pattern of sex-specific regulation following cohabitation, with a decrease in activity in males, but an increase in females—although such interaction did not reach significance for the citrate synthase measurements (citrate synthase: $F_{1,16} < 0.01$, $p = 0.982$ for Cohabitation, $F_{1,16} < 0.01$, $p = 0.960$ for Sex, and $F_{1,16} = 4.34$, $p = 0.054$ for the interaction, Fig. S7B; complex I-II junction: $F_{1,25} = 0.05$, $p = 0.825$ for Cohabitation, $F_{1,25} = 2.07$, $p = 0.162$ for Sex, and $F_{1,25} = 4.34$, $p = 0.048$ for the interaction, Fig. S7C). Interestingly, although overall activity levels for all other components of the electron transport chain measured

did not differ between groups (Fig. S7C, Table S5), we found a positive relation between cytochrome C activity and aggressive behaviors during the RIT in females but not in males (Fig. S7D,E), supporting a higher involvement of mitochondrial function in the NAc following 24 hrs of cohabitation in female than in male prairie voles.

Furthermore, despite the lack of group differences, cytochrome C activity was positively associated with the number of aggressive bouts during the RIT in females, but not males, thereby supporting a more prominent link in females than in males between mitochondrial activity and selective aggression. Although such a causal link remains to be verified, it is particularly interesting to note that mitochondrial respiration in the NAc mediates social hierarchy and anxiety in rats. Indeed, while high-anxious rats prone to become subordinate during a social encounter exhibit reduced mitochondrial respiration (as measured by complex I and II activity) in the NAc when compared to low-anxious rats, intra-NAc pharmacological inhibition of complexes I and II reduced social rank and mimicked high-anxious rats and boosting mitochondrial respiration prevented the development of social subordinance (103). Finally, D1R but not D2R activation in the NAc facilitates social dominance and mitochondrial respiration (104). Altogether, these data support an involvement of accumbal mitochondrial activity in the establishment and maintenance of a pair-bond in prairie voles and suggest a particular link in females with the development and/or expression of selective aggression.

Neuropeptides and dopamine systems

A variety of neurotransmitters and their receptors, including the oxytocin, vasopressin, and dopamine systems, have been involved in partner preference formation (1), although with sex-specific alterations of gene expression in the NAc. Indeed, while 24 hrs of cohabitation with mating up-regulate oxytocin receptors (OTR) and vasopressin V1a receptors (V1aR) in females, males show an increase in OTR but not V1aR (9,11). Notably, neither OTR nor V1aR mRNA levels show changes in the ventral striatum of male and female prairie voles pair-bonded for 2 weeks,

suggesting distinct mechanisms underlying pair-bond formation and its maintenance (5) and further supporting the sex- and cohabitation duration-specific regulation of gene expression observed in our study. In this study, while we do reproduce the lack of sex differences in OTR at baseline in the prairie vole NAc (75), no regulations of OTR or V1aR mRNA levels following cohabitation with a partner were detected, likely resulting from a substantial inter-individual variability commonly found in prairie voles at the behavioral and gene levels (see Fig. 1 for an illustration of within-group variability at the behavioral level). Notably, OTR and V1aR mRNA in particular exhibit substantial inter-individual differences in expression in the prairie vole brain resulting from single-nucleotide polymorphisms (76–80), which could thus participate to explain the variability in RNAseq counts observed in our study. Interestingly, however, we nonetheless found a significant enrichment of the oxytocin signaling pathway (KEGG pathway) supported by 18 genes up-regulated in females pair-bonded for 3 weeks when compared to pair-bonded males (Table S12) suggesting sex-specific overall regulations downstream of OTR towards a sustained oxytocin neurotransmission and signaling. While this hypothesis remains to be tested, it is interesting to note that higher oxytocin neurotransmission in female than male prairie voles has been suggested by early reports that intracerebroventricular injection of oxytocin facilitate partner preference formation in female but not male prairie voles (81,82). Although the latter studies did not detail the specificity of the NAc, they nevertheless represent interesting elements related to a sex-specific regulation of sensitivity of the oxytocin neurotransmission in prairie voles (for review, see (83)). In addition, recent evidence does further support an important regulation of OTR downstream signaling in the NAc in mediating social behaviors. Indeed, in the monogamous california mouse (*Peromyscus californicus*), the simultaneous activation of Gi-coupled OTR and blockade of Gq-coupled OTR reduces social approach. Conversely, activation of Gq-coupled OTR increases social approach (84), thereby revealing an opposite regulation of social behaviors depending on OTR downstream signaling.

Similar to OTR, no significant changes in V1aR mRNA levels were detected in our study, in contradiction with previous reports of V1aR up-regulation following 24 hrs but not 2 weeks of pair-bonding (5,11). Nevertheless, our gene network analyses revealed V1aR as one of the key driver genes ("hub" genes) in the yellow-orangered4-orange-tan group of modules (Fig. S15). Interestingly, this group of modules is positively associated with the expression of selective aggression during the RIT (Fig. S5). In this context, our current study does expand V1aR's involvement in the regulation of pair bonding in the male prairie vole NAc by suggesting an underlying network of genes (Fig. S15) contributing to V1aR's role in pair-bonding regulation.

Alongside changes in OTR and V1aR, regulation of dopamine release and its receptors in the NAc modulates pair bonding in prairie voles. While dopamine D1 receptors (D1R) promote the maintenance but inhibit the formation of the pair-bond, dopamine D2 receptors (D2R) inhibit its maintenance but promote its formation (7,105). Accordingly, two weeks of pair-bonding increase D1-like but not D2-like receptor binding in the male NAc (7), as well as D1R but not D2R mRNA levels in both the male and female ventral striatum (5). Notably, electrically evoked dopamine release in the NAc is enhanced by pair bonding in prairie voles, but to a greater extent in females than in males (5), thereby highlighting an overall modulation of dopaminergic transmission occurring in pair-bonded prairie voles, but to a greater extent in females than males. Although we did not detect a significant increase in D1R mRNA in males following pair-bonding (Table S10), we did detect higher D1R, as well as D2R, mRNA levels in females than males following three weeks of cohabitation with a partner, in line with the enhanced modulation of dopaminergic neurotransmission in pair-bonded females previously reported (5). Interestingly, a similar female bias at the 3W timepoint was observed for a variety of genes related to dopaminergic transmission and signaling (Table S6), which thus supports an overall sex-biased modulation of dopaminergic transmission in the later phase of the pair-bonding process.

Sex-biased regulation of genes linked to autism spectrum disorders (ASD)

Due to their highly social nature, prairie voles represent an excellent animal model to study the neurobiology underlying dysfunctions in social behaviors such as those seen in autism spectrum disorders (ASD)(95). Interestingly, impairments in synaptic plasticity constitute core components of ASD pathogenesis, and extensive genetic and whole-exome studies identified hundreds of genes—in its March 4th, 2020 release, the SFARI Gene database (41,42) includes 913 genes—related to synaptic plasticity through DNA transcription, RNA translation, protein degradation, as well as synaptic organization as ASD risk genes (96–99). In light of the similarities between these pathways and those found affected following pair-bonding in our dataset, we tested whether ASD-linked genes would be enriched in the differentially expressed genes in our dataset. Moreover, 826 out of the 913 genes in the SFARI Gene database were also detected in our dataset (regardless of their differentially expressed status, Table S11), confirming a sufficient overlap between the two datasets for functional enrichment analyses. Across all comparisons, we thus found a significant enrichment of ASD-linked genes in the sexually-biased genes at baseline and at 3W (Fig. S18, Table S11). As in our main dataset, the two sets of genes only partially overlap, indicating that the set of ASD-linked sexually-biased genes following 3 weeks of cohabitation in the prairie vole NAc differ from baseline (Fig. S18B). In line with the broad enrichment of pathways in the sexually-biased genes at baseline and 3W (Fig. 5), a functional analysis of ASD-linked sexually-biased genes at these timepoints revealed a strong enrichment of processes, molecular functions, cellular components, and pathways closely related to neurotransmission and neuroplasticity (Fig. S19, Table S13). Among these processes and pathways, it is particularly interesting to find the up-regulation of genes related to D1R binding in 3W females when compared to 3W males, carried by the *Dlg4* (PSD-95), *Ptpn11* (SHP-2), and *Ppp1r1b* (DARPP-32) (Fig. S19, Table S13). In striatal neurons, PSD-95 can bind D1R and negatively regulate its downstream signaling activity (91–93), but a role for PSD-95 in promoting D1R recycling and resensitization has also been reported (94). In striatal primary cultures, the

tyrosine phosphatase SHP-2 interacts with D1R and is required for D1R-induced ERK1/2 activation (95). Finally, DARPP-32 is a major regulator of dopamine-induced intracellular signaling and plays a role in response to reward, including in a social context (for review, see (96)). Combined with the enhanced increase in dopamine release observed in female prairie voles following pair-bonding when compared to males (5), the female-biased up-regulation of these genes provides interesting novel candidates in mediating pair-bond maintenance in the monogamous prairie voles.

Evaluation of monogamy candidate genes

Recently, a transcriptomic comparison between monogamous and non-monogamous species revealed a shared profile of gene expression in the brain across vertebrates, including voles (97). Notably, these monogamy candidate genes functionally relate to DNA transcription as well as neurotransmission and synaptic receptor signaling in particular (97), all biological processes and functions enriched following cohabitation with a partner in our dataset. Even though these monogamy candidate genes were established from the combined forebrain and midbrain tissues of male individuals only, we thus sought to evaluate their regulation in our dataset. Out of the 42 monogamy candidate genes (97), 40 were detected in our dataset, 7 of which being classified as differentially expressed in at least one comparison: *Dscam*, *Lpar1*, *Mast4*, *Kmt2c*, *Ctnna1*, *Dpysl4*, and *Pik3r2* (Fig. S20). While most of these only are sexually-biased at baseline and/or following cohabitation with a partner (*Mast4*, *Lpar1*, *Dscam*, *Ctnna*, and *Pik3r2*), others (*i.e. Dpysl4* and *Kmt2c*) interestingly are modulated in the early phase of the pair-bonding process (24H) in males (Fig. S20). In mice, DPYSL4 (also known as CRMP3) is highly expressed in the hippocampus and is an important regulator of dendritic arborization (106) with additional neuroprotective effects against excitotoxicity (107). In addition, DPYSL4 has histone H4 deacetylase activity (108), which, in light of the enrichment of epigenetic regulation-related processes in our dataset (Fig. 4, Fig. 5) could represent an important regulator of neuroplasticity

in the prairie vole NAc following cohabitation with a partner. Similarly, KMT2C is an important epigenetic regulator through its histone methyltransferase activity and has been implicated in intellectual disability and ASD (109). In the prairie vole NAc, *Dpysl4* and *Kmt2c* mRNA levels were up- and down-regulated, respectively, in males at the early timepoint (24H), before returning to baseline at 3W. In light of their ability to epigenetically regulate gene expression, it is possible to hypothesize their involvement in the second wave of gene expression we observed in males at the 3W timepoint.

Supplementary Figures

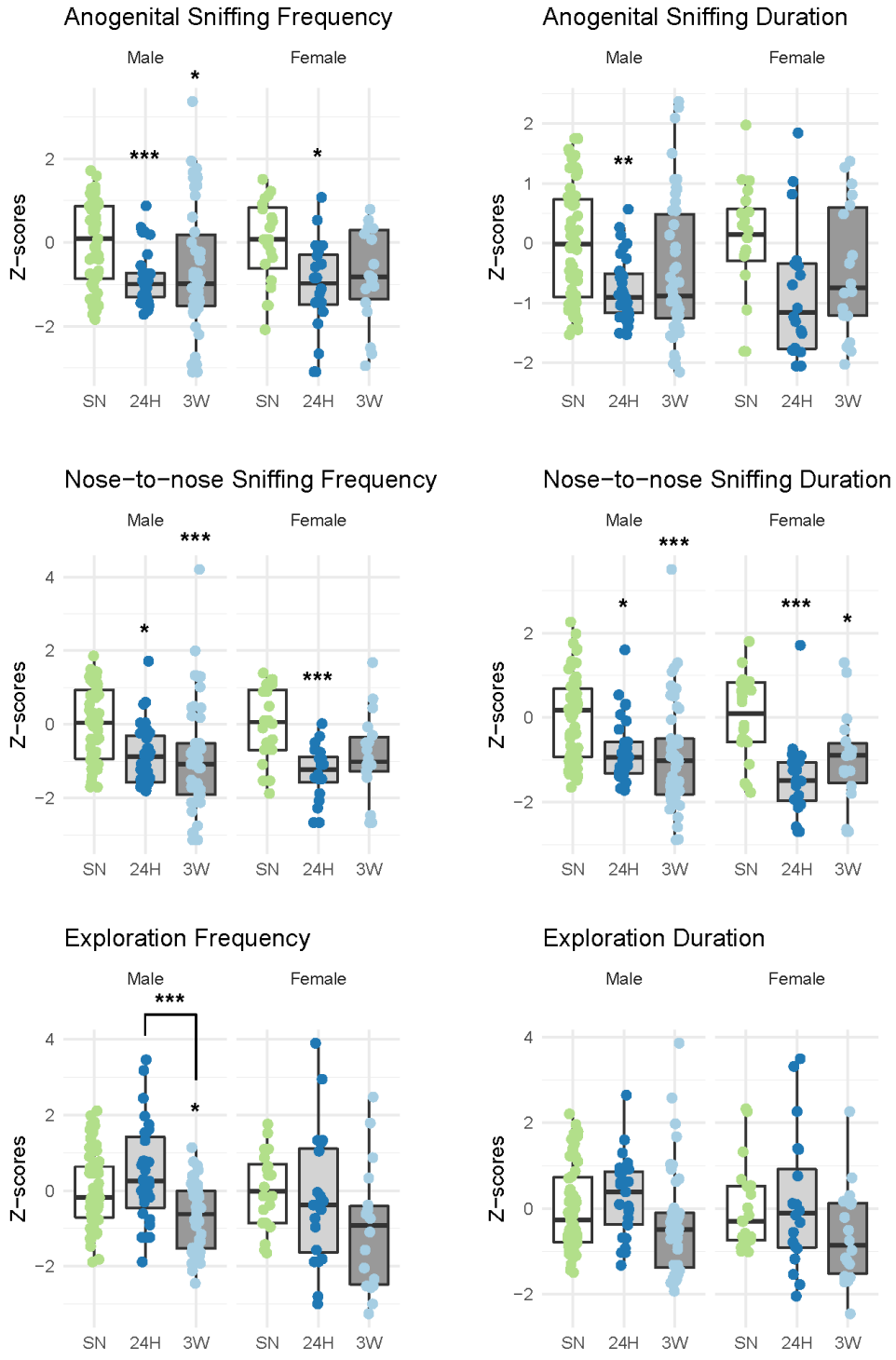

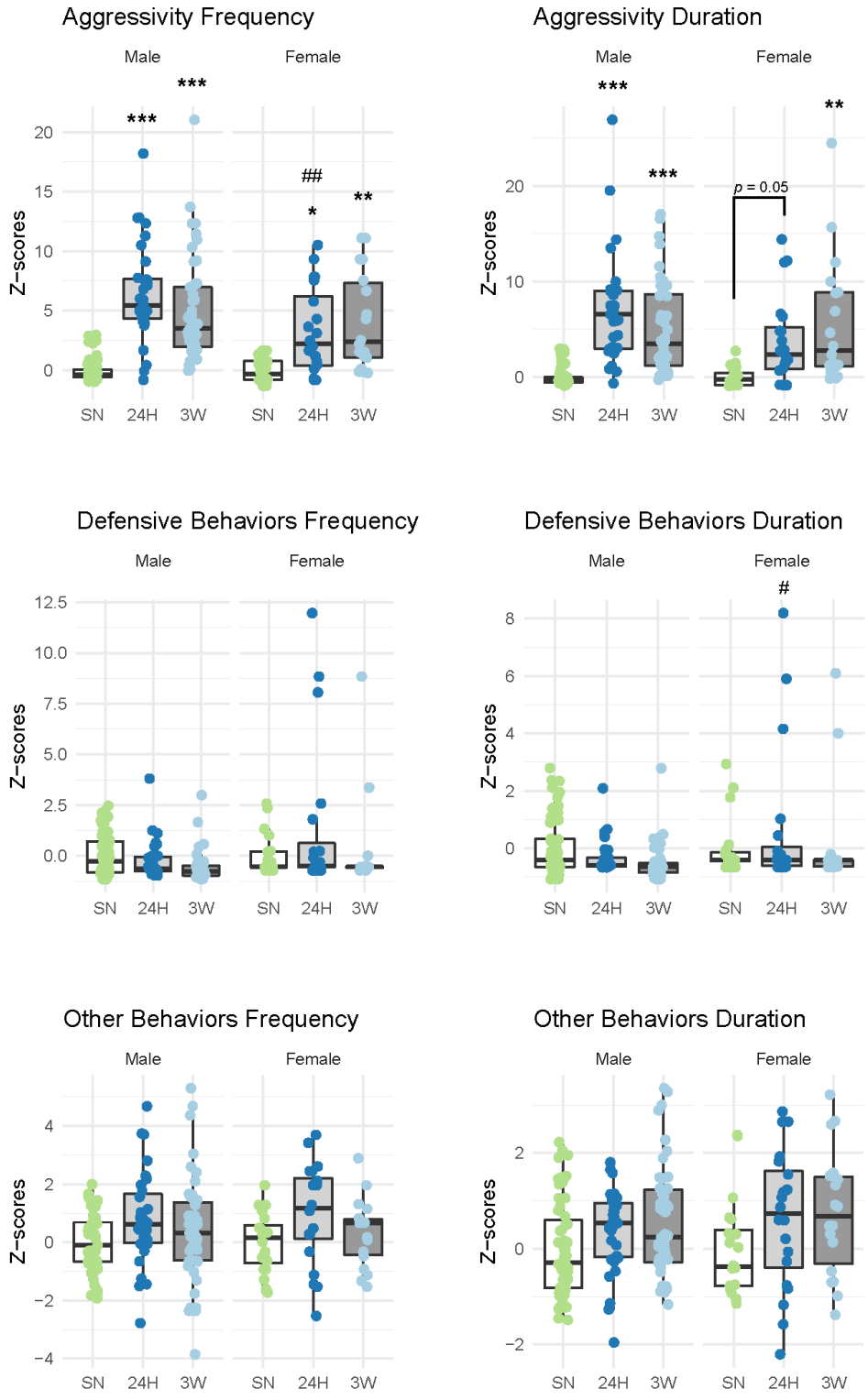
Aggressivity Frequency
Male
Female
Z−scores
SN 24H 3W SN 24H 3W
Aggressivity Duration
p = 0.05
Defensive Behaviors Frequency
Defensive Behaviors Duration
Other Behaviors Frequency
Other Behaviors Duration

Figure S1. Characterization of behaviors of male and female prairie voles in the resident-intruder test (RIT). Adult male and female prairie voles were cohabitated with a same-sex littermate (SN), or an opposite-sex partner for 24 hrs (24H) or 3 weeks (3W) before being subjected to a 10-min RIT. All behaviors frequencies (number of bouts) as well as durations were scored and normalized by z-scoring within cohorts and then between sexes. All data were analyzed using two-way ANOVA with Group (SN, 24H, 3W) and Sex as independent factors; all statistical values are reported in the enclosed table. Aggr: aggression behaviors, ano: anogenital sniffing, def: defensive behaviors, nose2nose: nose-to-nose sniffing, rest: others.

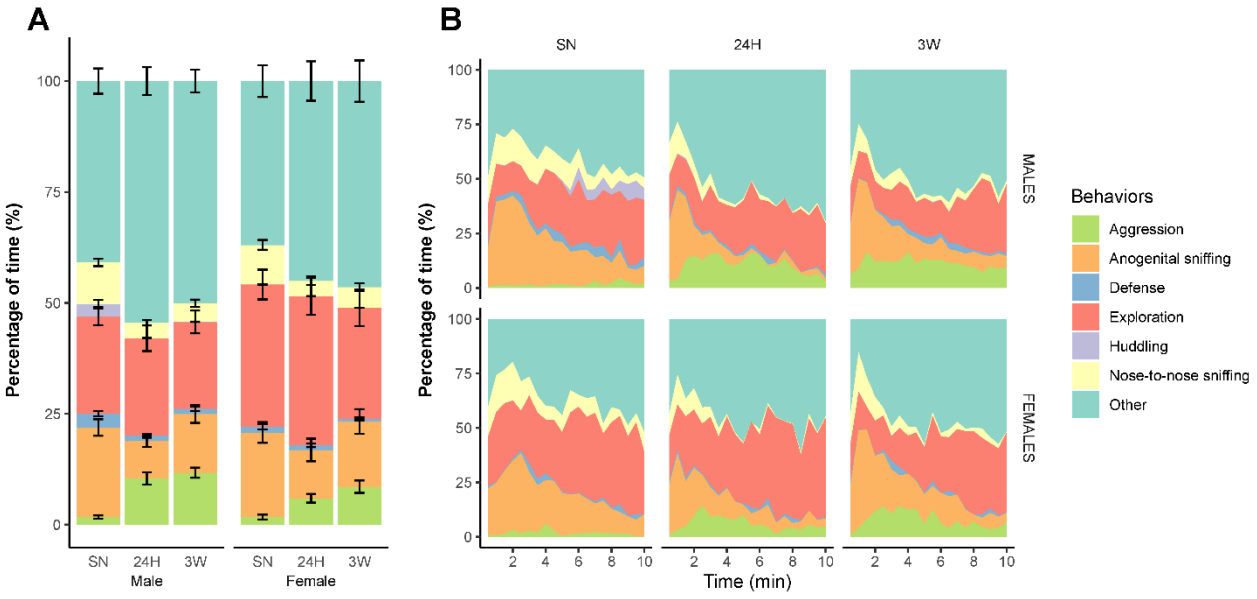

Figure S2. Distribution of time spent in each behavior during the resident-intruder test (RIT). Adult male and female prairie voles were cohabitated with a same-sex littermate (SN), or an opposite-sex partner for 24 hrs (24H) or 3 weeks (3W) before being subjected to a 10-min RIT. The percentage of time spent in each scored behavior is represented stacked over the entire 10-min session in (A), or across 30 sec timebins in (B).

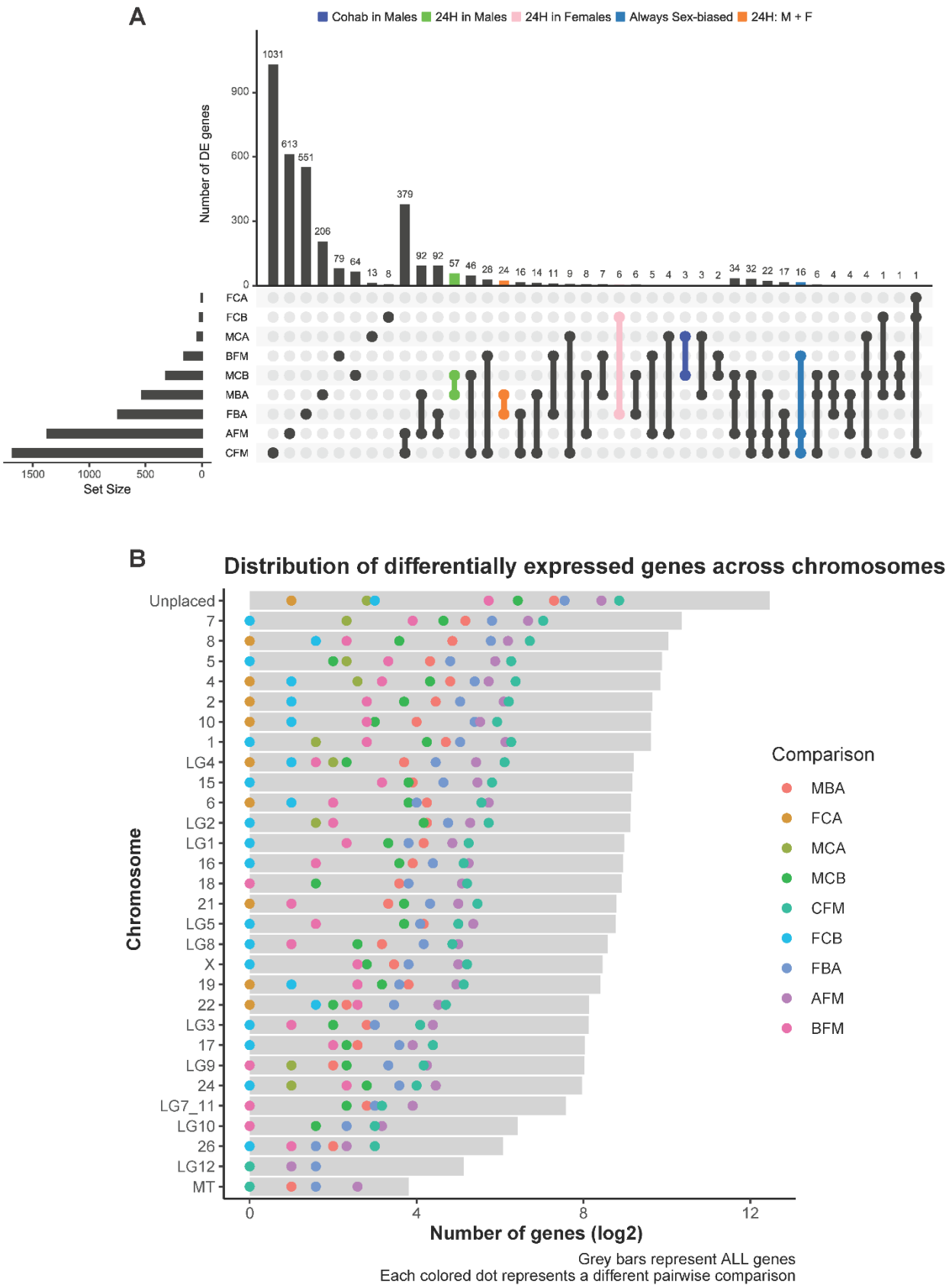
A
Cohab in Males
24H in Males
24H in Females
Always Sex-biased
24H: M + F
Number of DE genes
1031
613
551
206
79
64
13
8
379
92
92
57
46
28
24
16
14
11
9
8
7
6
6
5
4
3
3
2
34
32
22
17
16
6
4
4
4
1
1
1
FCA
FCB
MCA
BFM
MCB
MBA
FBA
AFM
CFM
1500
1000
500
0
Set Size
B
Distribution of differentially expressed genes across chromosomes
Chromosome
Unplaced
7
8
5
4
2
10
1
LG4
15
6
LG2
LG1
16
18
21
LG5
LG8
X
19
22
LG3
17
LG9
24
LG7_11
LG10
26
LG12
MT
0
4
8
12
Number of genes (log2)
Comparison
MBA
FCA
MCA
MCB
CFM
FCB
FBA
AFM
BFM
Grey bars represent ALL genes
Each colored dot represents a different pairwise comparison

Figure S3. Overlap in differential expression and chromosomes distribution. (A) UpSet plot depicting the intersections in differentially expressed genes between all sets of differentially expressed genes. Intersects of interest were manually colored for emphasis. M: Males, F: Females. (B) Representation of the number of differentially expressed genes across all chromosomes and linkage groups in the prairie vole assembly.

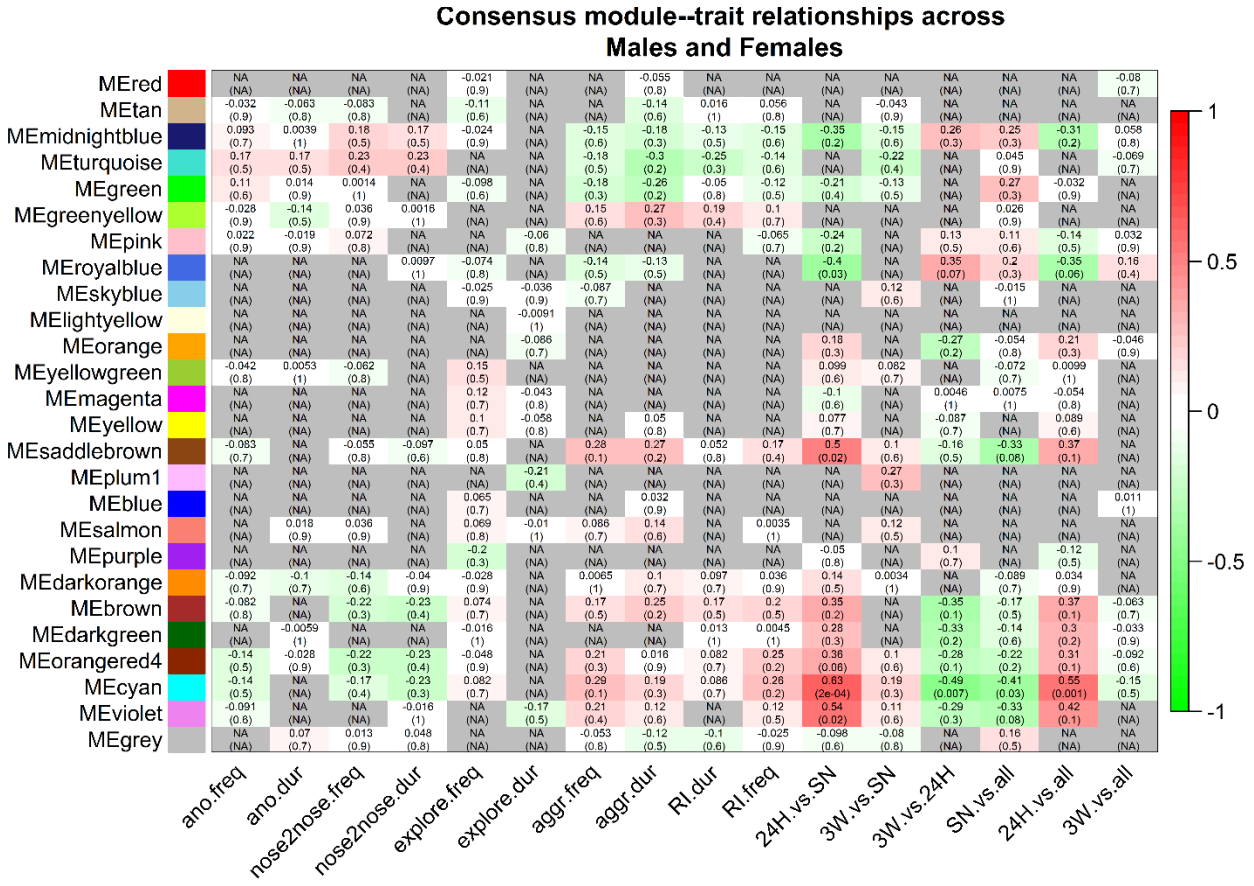

Figure S4. Consensus module-trait relationship across males and females. The consensus module-trait relationship was determined using the following conservative method, as recommended by the WGCNA authors. For each module-trait pair, the correlation with the lower absolute in the male and female set was chosen if the two correlations have the same sign, or zero relationship ("NA" in the figure) if the two correlations have opposite signs.

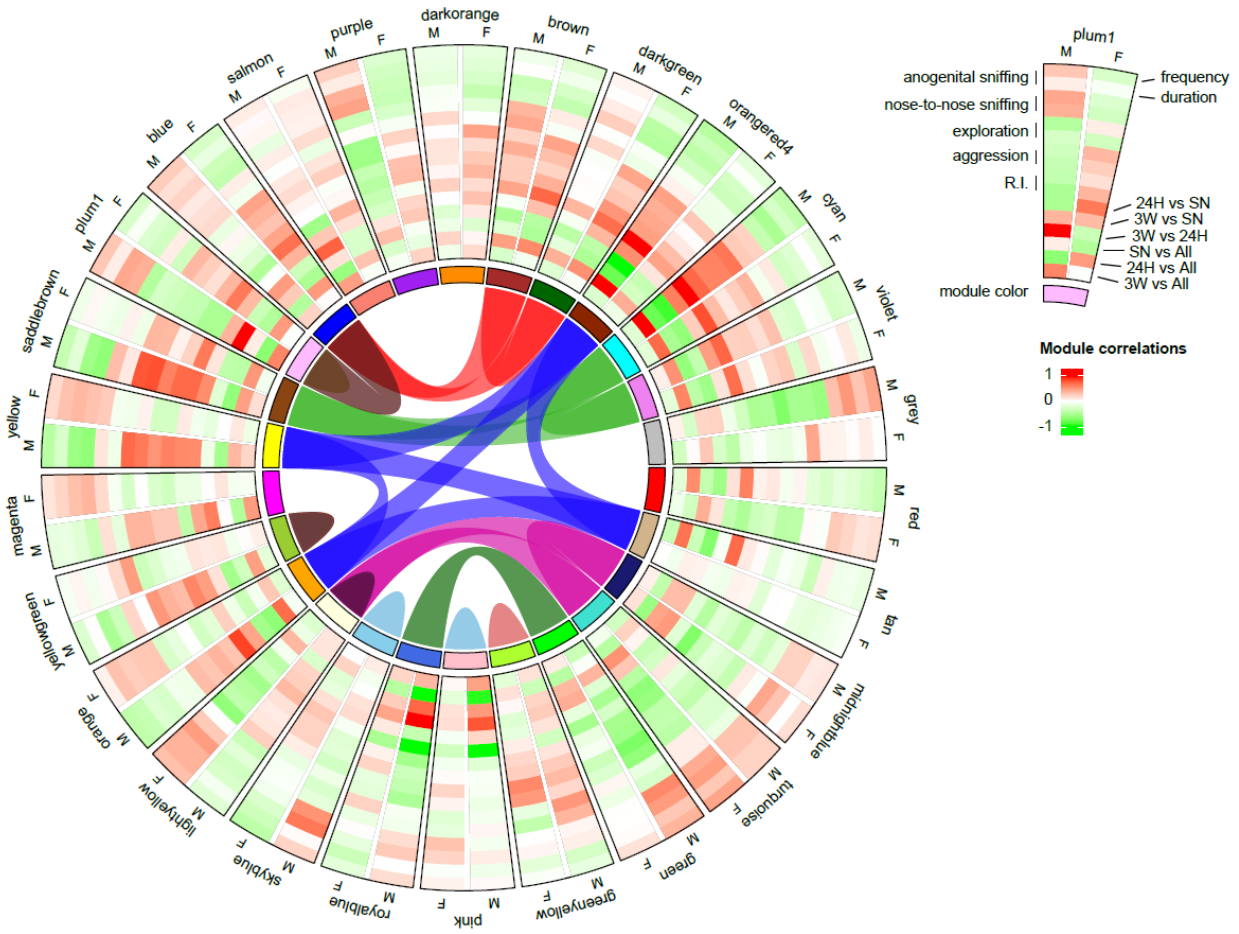

Figure S5. Sex-specific recruitment of gene co-expression modules following cohabitation with an opposite-sex partner in prairie voles. Circular plot comparing between males and females the correlation of each gene co-expression module of interest with each behavioral trait. While the inner circle depicts the module's color, the outer layers detail their correlation with each behavioral trait in males (M) and females (M) side-by-side. Modules showing similar patterns of correlations between males and females (male-specific, female-specific, common, or opposed) were grouped together (inner ribbons). These groups of modules of interest were further connected together when sharing directionality of relation with behavioral traits. R.I.: Resident-Intruder score.

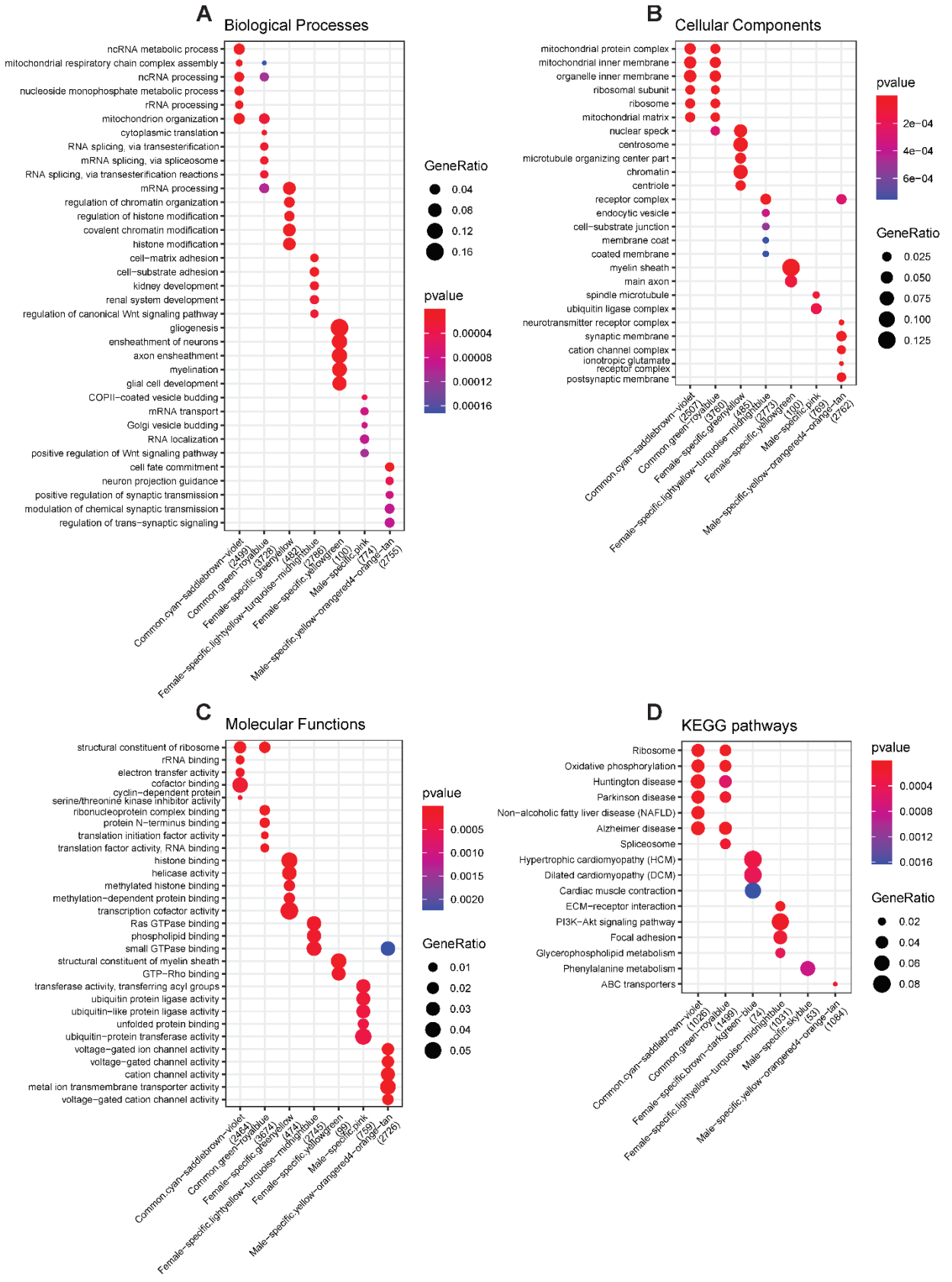
A
Biological Processes
ncRNA metabolic process
mitochondrial respiratory chain complex assembly
ncRNA processing
nucleoside monophosphate metabolic process
rRNA processing
mitochondrion organization
cytoplasmic translation
RNA splicing, via transesterification
mRNA splicing, via spliceosome
RNA splicing, via transesterification reactions
mRNA processing
regulation of chromatin organization
regulation of histone modification
covalent chromatin modification
histone modification
cell−matrix adhesion
cell−substrate adhesion
kidney development
renal system development
regulation of canonical Wnt signaling pathway
gliogenesis
ensheathment of neurons
axon ensheathment
myelination
glial cell development
COPII−coated vesicle budding
mRNA transport
Golgi vesicle budding
RNA localization
positive regulation of Wnt signaling pathway
cell fate commitment
neuron projection guidance
positive regulation of synaptic transmission
modulation of chemical synaptic transmission
regulation of trans−synaptic signaling
Common.cyan−saddlebrown−violet (2499)
Common.green−royalblue (3728)
Female−specific.greenyellow (482)
Female−specific.lightyellow−turquoise−midnightblue (2786)
Female−specific.yellowgreen (100)
Male−specific.pink (774)
Male−specific.yellow−orangered4−orange−tan (2755)
GeneRatio
0.04
0.08
0.12
0.16
pvalue
0.00004
0.00008
0.00012
0.00016
B
Cellular Components
mitochondrial protein complex
mitochondrial inner membrane
organelle inner membrane
ribosomal subunit
ribosome
mitochondrial matrix
nuclear speck
centrosome
microtubule organizing center part
chromatin
centriole
receptor complex
endocytic vesicle
cell−substrate junction
membrane coat
coated membrane
myelin sheath
main axon
spindle microtubule
ubiquitin ligase complex
neurotransmitter receptor complex
synaptic membrane
cation channel complex
ionotropic glutamate receptor complex
postsynaptic membrane
Common.cyan−saddlebrown−violet (2507)
Common.green−royalblue (3760)
Female−specific.greenyellow (485)
Female−specific.lightyellow−turquoise−midnightblue (2773)
Female−specific.yellowgreen (101)
Male−specific.pink (769)
Male−specific.yellow−orangered4−orange−tan (2762)
pvalue
2e−04
4e−04
6e−04
GeneRatio
0.025
0.050
0.075
0.100
0.125
C
Molecular Functions
structural constituent of ribosome
rRNA binding
electron transfer activity
cofactor binding
cyclin−dependent protein serine/threonine kinase inhibitor activity
ribonucleoprotein complex binding
protein N−terminus binding
translation initiation factor activity
translation factor activity, RNA binding
histone binding
helicase activity
methylated histone binding
methylation−dependent protein binding
transcription cofactor activity
Ras GTPase binding
phospholipid binding
small GTPase binding
structural constituent of myelin sheath
GTP−Rho binding
transferase activity, transferring acyl groups
ubiquitin protein ligase activity
ubiquitin−like protein ligase activity
unfolded protein binding
ubiquitin−protein transferase activity
voltage−gated ion channel activity
voltage−gated channel activity
cation channel activity
metal ion transmembrane transporter activity
voltage−gated cation channel activity
Common.cyan−saddlebrown−violet (2464)
Common.green−royalblue (3674)
Female−specific.greenyellow (474)
Female−specific.lightyellow−turquoise−midnightblue (2745)
Female−specific.yellowgreen (99)
Male−specific.pink (759)
Male−specific.yellow−orangered4−orange−tan (2726)
pvalue
0.0005
0.0010
0.0015
0.0020
GeneRatio
0.01
0.02
0.03
0.04
0.05
D
KEGG pathways
Ribosome
Oxidative phosphorylation
Huntington disease
Parkinson disease
Non−alcoholic fatty liver disease (NAFLD)
Alzheimer disease
Spliceosome
Hypertrophic cardiomyopathy (HCM)
Dilated cardiomyopathy (DCM)
Cardiac muscle contraction
ECM−receptor interaction
PI3K−Akt signaling pathway
Focal adhesion
Glycerophospholipid metabolism
Phenylalanine metabolism
ABC transporters
Common.cyan−saddlebrown−violet (1026)
Common.green−royalblue (1498)
Female−specific.brown−darkgreen−blue (74)
Female−specific.lightyellow−turquoise−midnightblue (1031)
Male−specific.skyblue (53)
Male−specific.yellow−orangered4−orange−tan (1084)
pvalue
0.0004
0.0008
0.0012
0.0016
GeneRatio
0.02
0.04
0.06
0.08

Figure S6. Functional enrichment in groups of modules of interest. For each group of modules of interest, the functional enrichment in gene ontologies from the biological processes (A), cellular components (B), and molecular functions (C) were tested, along with KEGG pathways (D) enrichments.

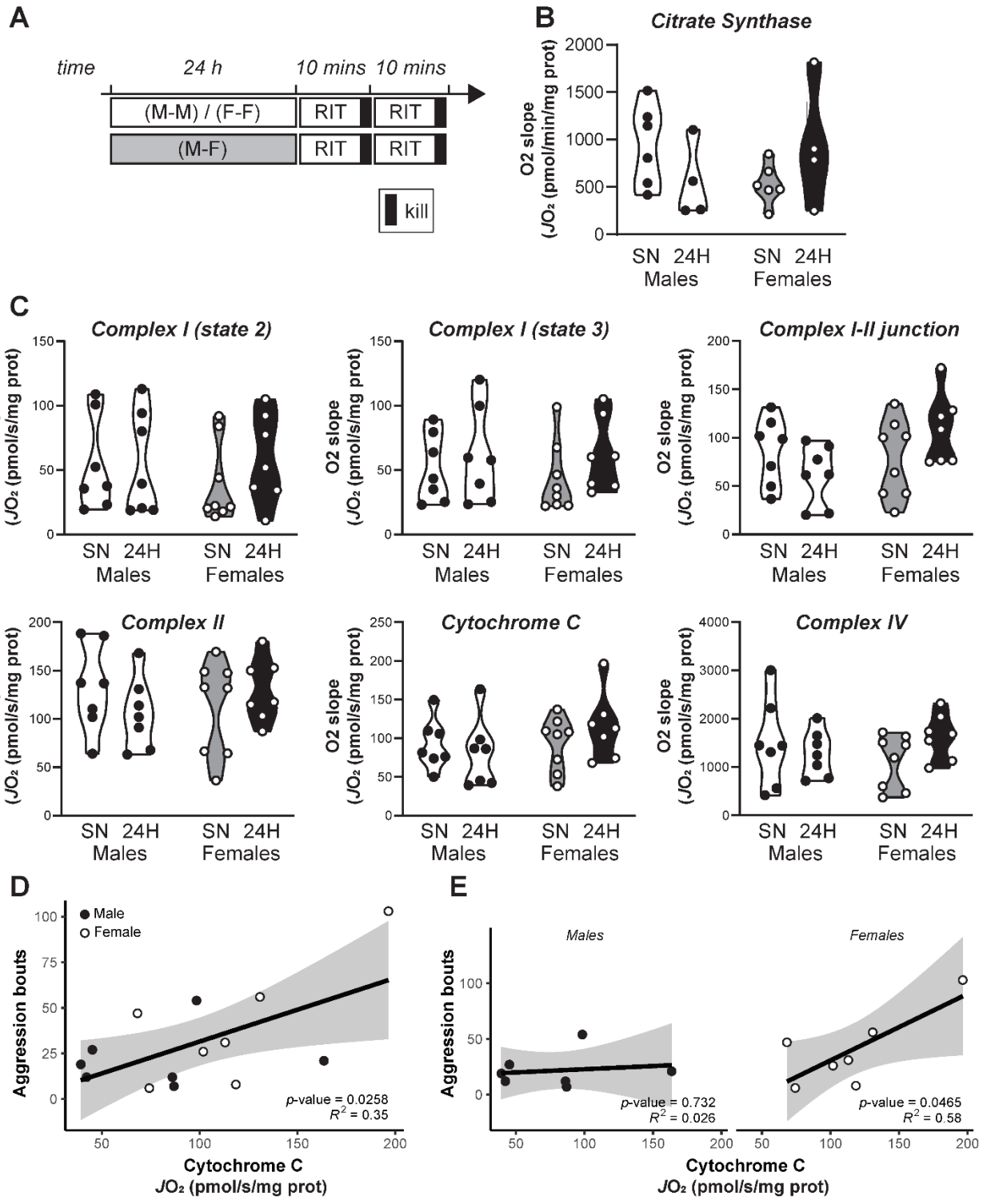

Figure S7. Analysis of mitochondrial activity in the nucleus accumbens following 24 hrs of cohabitation. (A) Adult male (M) and female (F) prairie voles were cohabitated for 24 hrs with a same sex littermate or opposite-sex partner for 24 hrs, before being subjected to a Resident-

Intruder Test (RIT). Immediately after RIT, the test subject was killed, and tissue punches from the nucleus accumbens were freshly collected and processed within hours for measurement of mitochondrial activity by high-resolution respirometry. Citrate synthase (B), as well as complex I (state 2), complex I (state 3), complex I-II junction, complex II, cytochrome C, and complex IV were thus measured (C). Notably, cytochrome C measurements showed a positive link with the number of aggressive bouts displayed during the RIT in voles cohabitated with an opposite-sex partner (D), which was carried by females but not males (E).

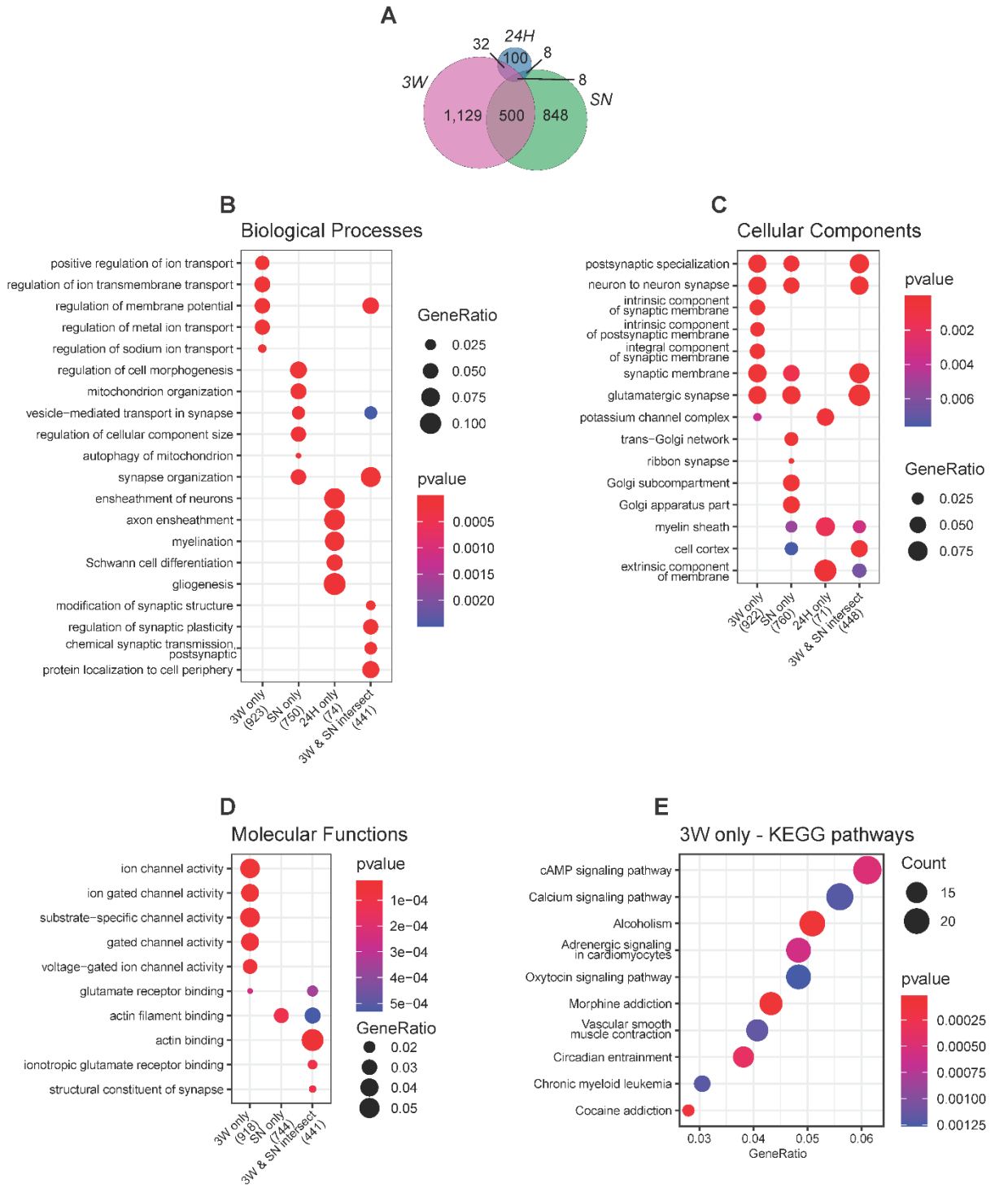

Figure S8. Functional enrichment of common and unique sexually-biased genes in the prairie vole nucleus accumbens. (A) As presented in Fig. 2, this euler diagram depicts the overlap between all three sets of sexually-biased genes: in sexually-naive controls (SN), as well as after

24 hrs (24H) or 3 weeks (3W) of cohabitation with an opposite-sex partner. For each set, the functional enrichment in gene ontologies of the biological processes (B), cellular components (C), and molecular functions (D) was tested. In addition, the functional enrichment in KEGG pathways for the sexually-biased genes following 3 weeks of cohabitation with an opposite-sex partner only is depicted in (E).

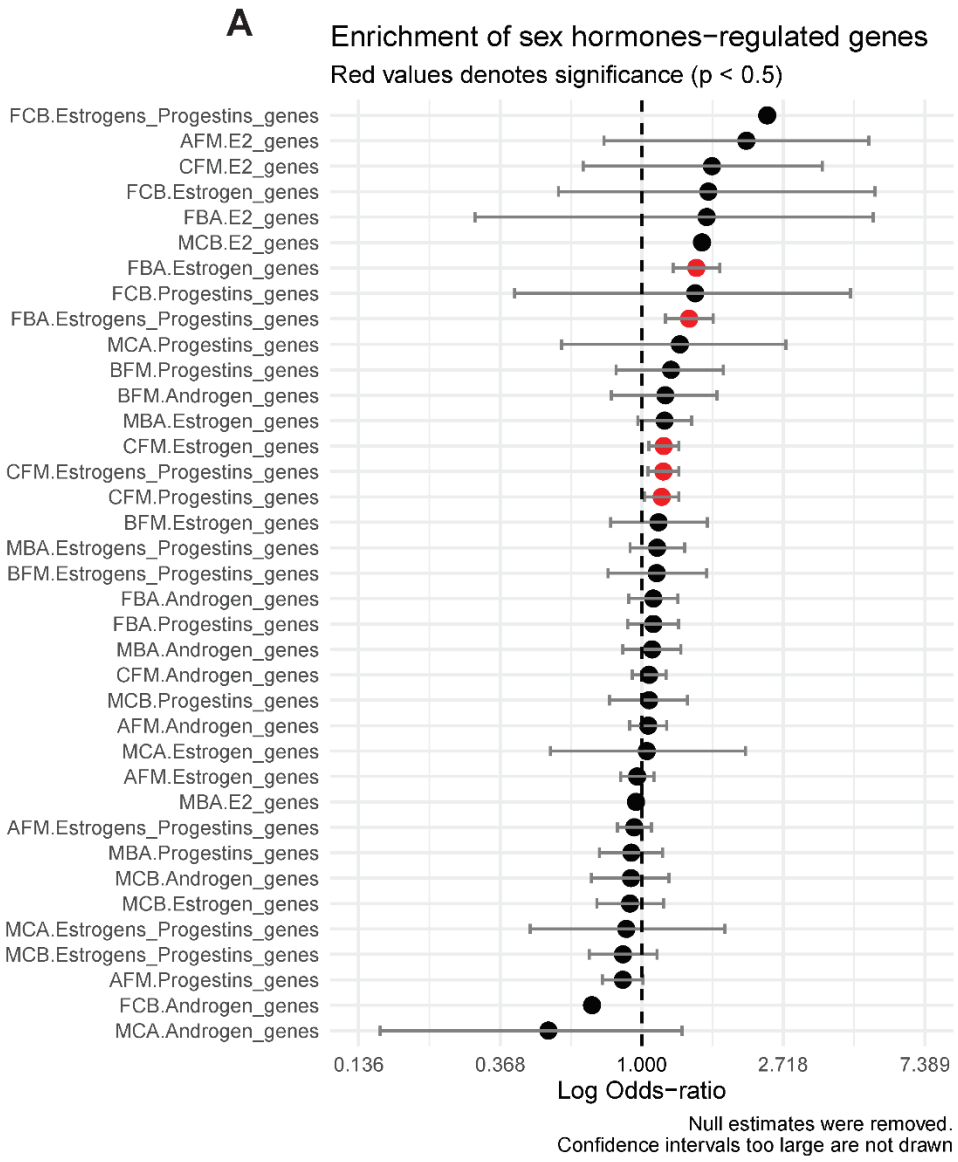
A
Enrichment of sex hormones−regulated genes
Red values denotes significance (p < 0.5)
FCB.Estrogens_Progestins_genes
AFM.E2_genes
CFM.E2_genes
FCB.Estrogen_genes
FBA.E2_genes
MCB.E2_genes
FBA.Estrogen_genes
FCB.Progestins_genes
FBA.Estrogens_Progestins_genes
MCA.Progestins_genes
BFM.Progestins_genes
BFM.Androgen_genes
MBA.Estrogen_genes
CFM.Estrogen_genes
CFM.Estrogens_Progestins_genes
CFM.Progestins_genes
BFM.Estrogen_genes
MBA.Estrogens_Progestins_genes
BFM.Estrogens_Progestins_genes
FBA.Androgen_genes
FBA.Progestins_genes
MBA.Androgen_genes
CFM.Androgen_genes
MCB.Progestins_genes
AFM.Androgen_genes
MCA.Estrogen_genes
AFM.Estrogen_genes
MBA.E2_genes
AFM.Estrogens_Progestins_genes
MBA.Progestins_genes
MCB.Androgen_genes
MCB.Estrogen_genes
MCA.Estrogens_Progestins_genes
MCB.Estrogens_Progestins_genes
AFM.Progestins_genes
FCB.Androgen_genes
MCA.Androgen_genes
0.136
0.368
1.000
2.718
7.389
Log Odds−ratio
Null estimates were removed.
Confidence intervals too large are not drawn

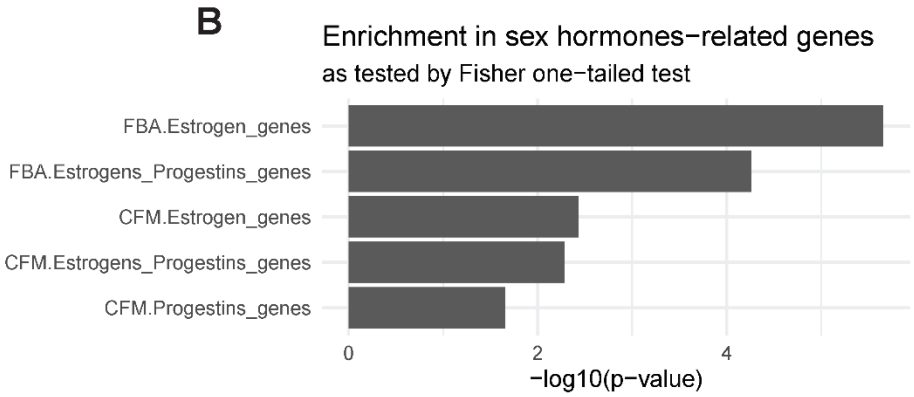
B
Enrichment in sex hormones−related genes
as tested by Fisher one−tailed test
FBA.Estrogen_genes
FBA.Estrogens_Progestins_genes
CFM.Estrogen_genes
CFM.Estrogens_Progestins_genes
CFM.Progestins_genes
0
2
4
−log10(p−value)

Figure S9. Enrichment of sex hormones-responsive genes. (A) The enrichment in known sex-hormones responsive genes was tested in all sets of differentially expressed genes and depicted as log of the corresponding odd-ratio. Note that null estimates were excluded from the plot, and that significant enrichments ($p < 0.05$) are highlighted in red. In (B), the -log10 of the *p*-value for all significant enrichments are detailed.

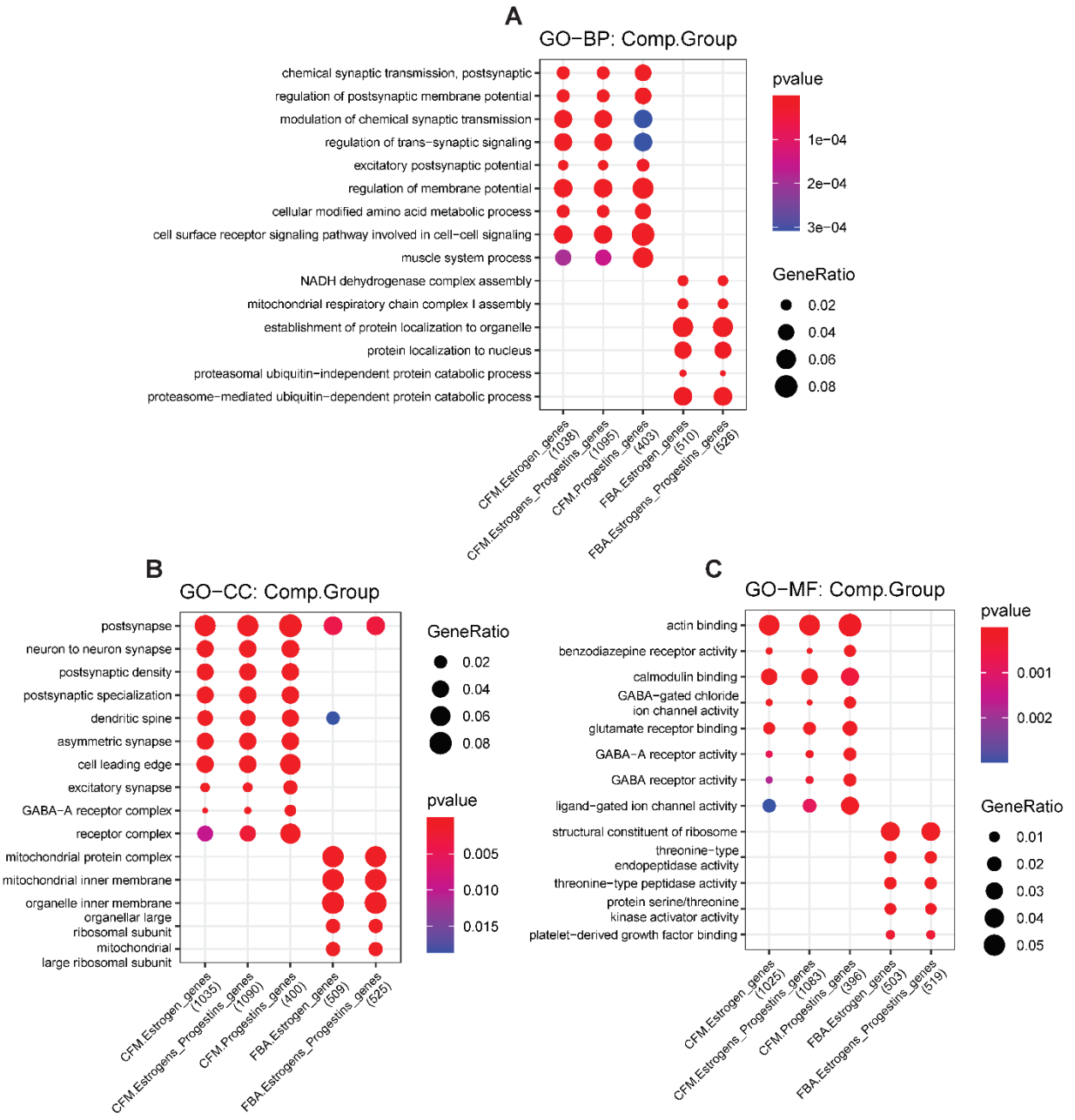

Figure S10. Functional analysis of significantly enriched sex hormones-responsive genes. Gene ontology enrichments were tested in each set of sex hormones-responsive genes against the biological processes (GO-BP, A), cellular components (GO-CC, B), and molecular functions (GO-MF, C) categories.

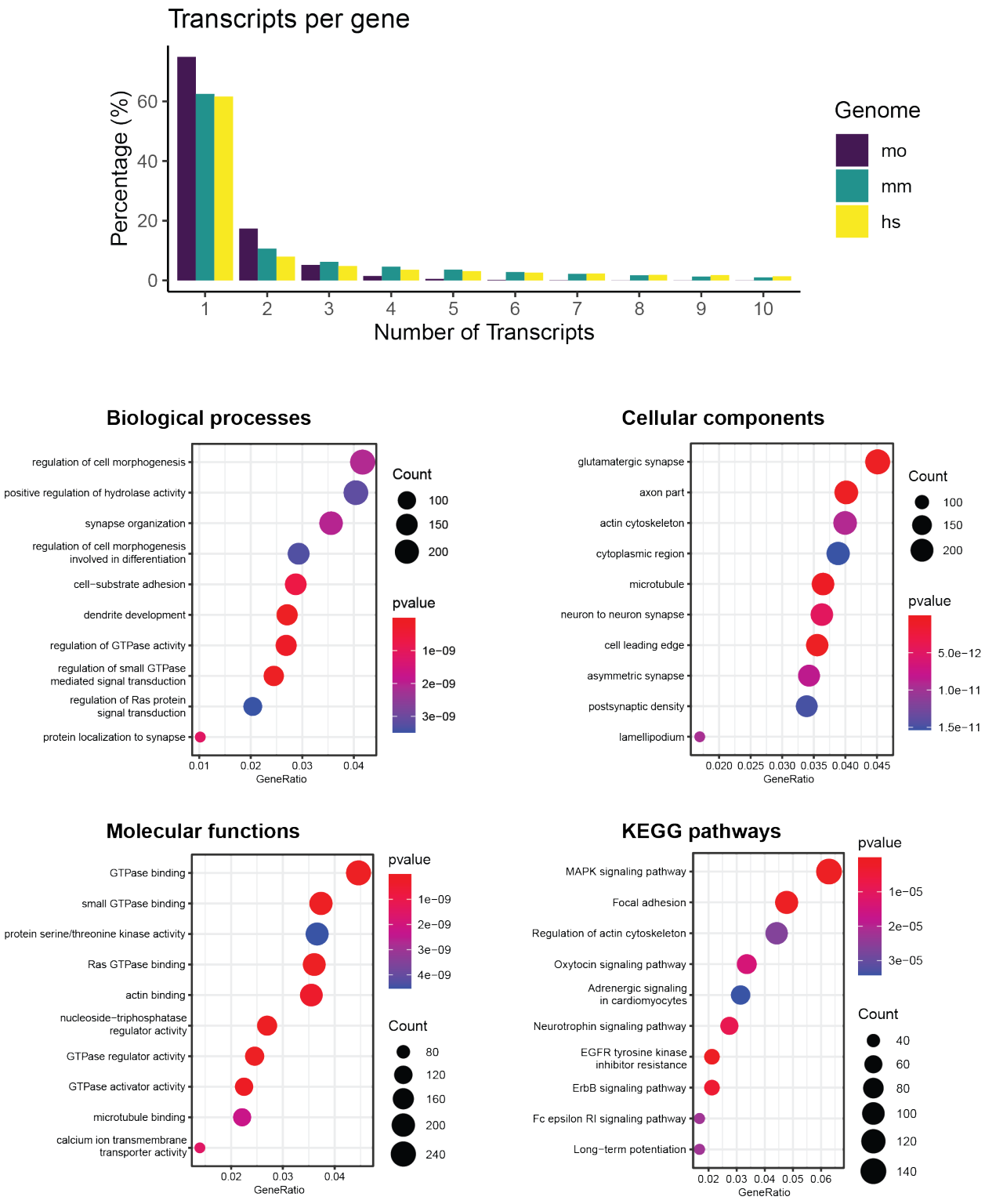

Figure S11. Analysis of multi-transcripts genes in the prairie vole genome. The top panel depicts the percentage of genes in prairie vole (*Microtus ochrogaster*, mo), mouse (*Mus musculus*, mm), and human (*Homo sapiens*, hs) genomes with 1–10 annotated transcripts. The bottom four panels

summarize the gene ontology enrichments of all prairie voles genes with two or more transcripts against the biological processes, cellular components, and molecular functions categories, as well as KEGG pathways.

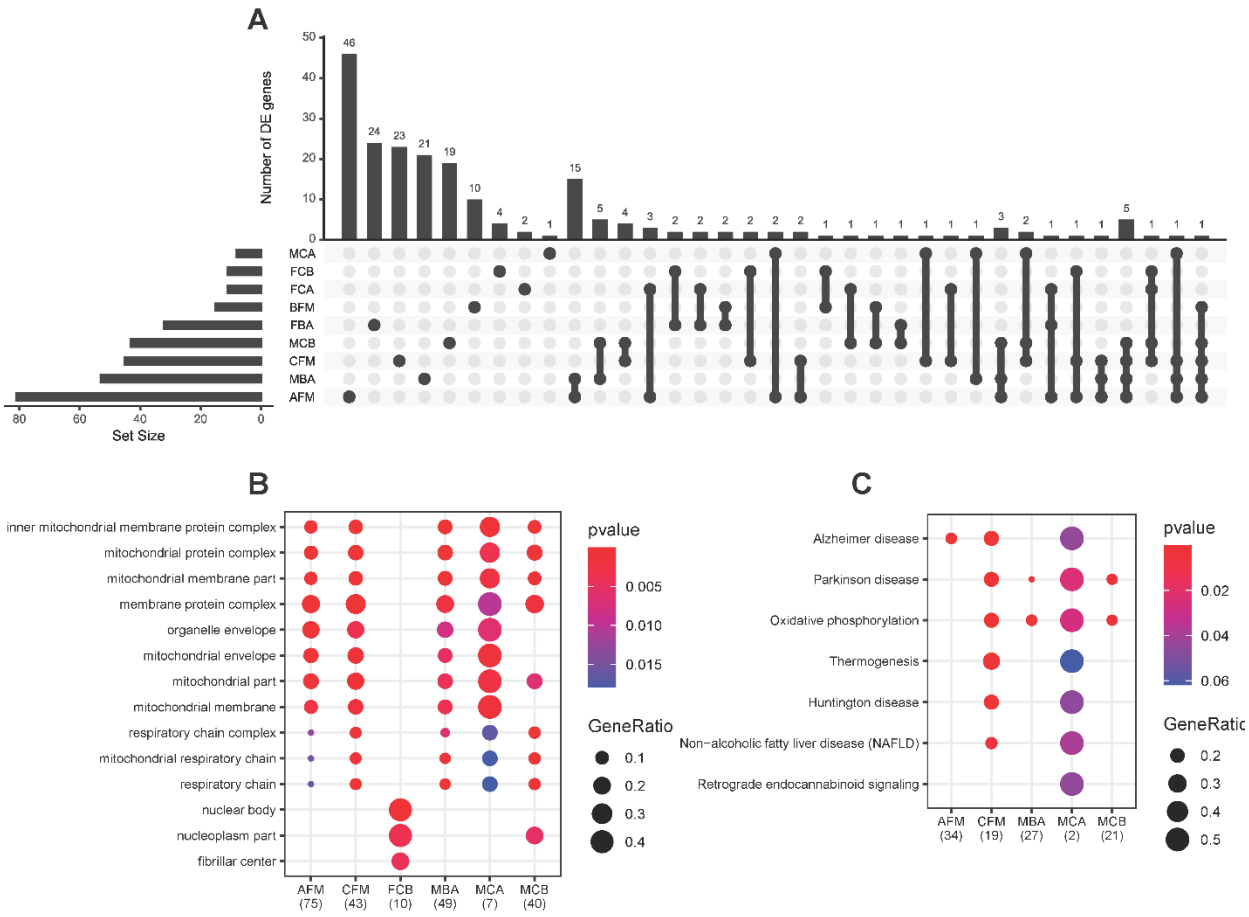

Figure S12. Overlap and functional analysis of genes with differential transcript usage. (A) UpSet plot depicting the intersections in genes with differential transcript usage between all sets of pairwise comparisons. Functional enrichment of gene ontology (cellular components, B) and KEGG pathways (C) in genes with differential transcript usage.

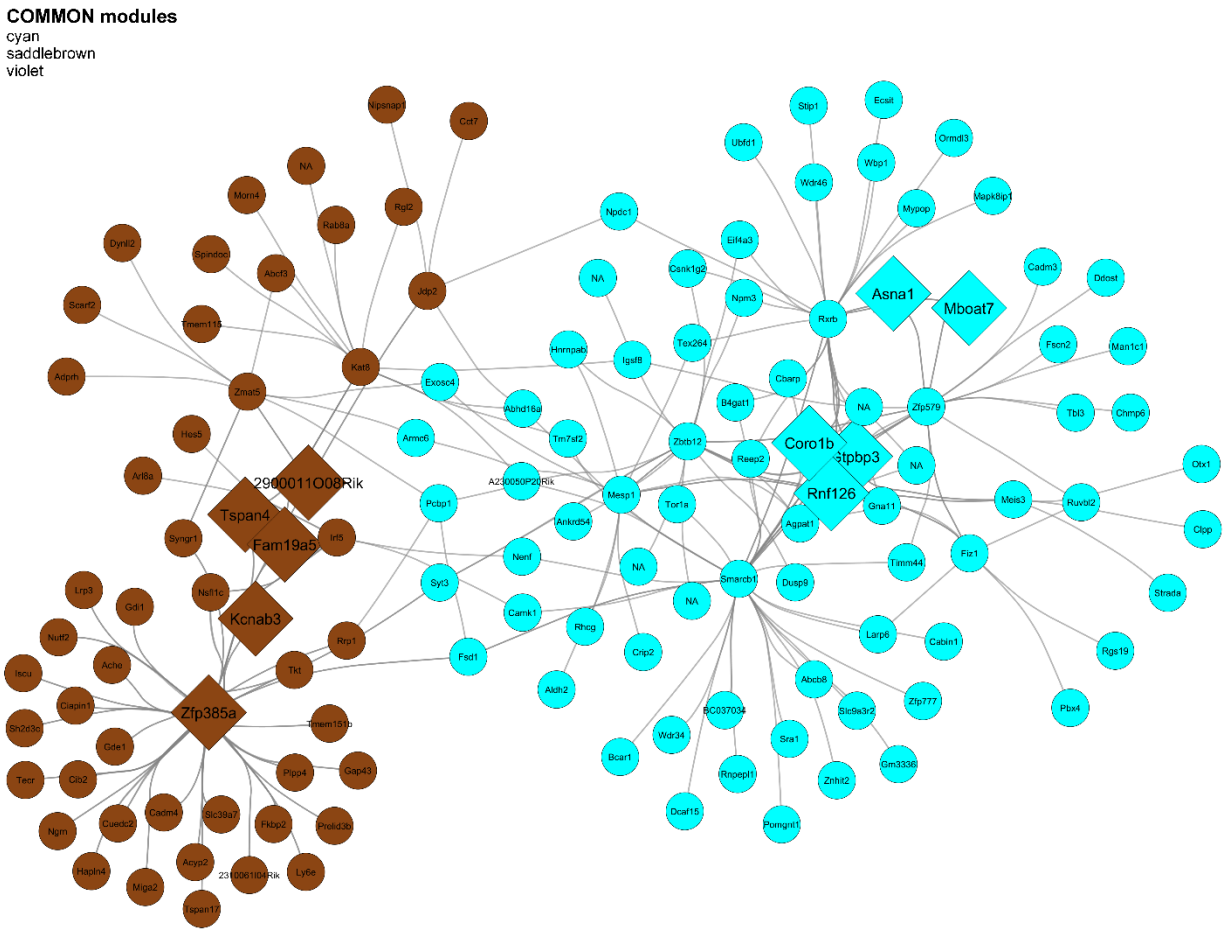

Figure S13. Gene interactions network for the common group of modules cyan-violet-saddlebrown. Each node corresponds to a gene and is colored according to its module. All genes detected as “hub genes” are represented with a diamond shape.

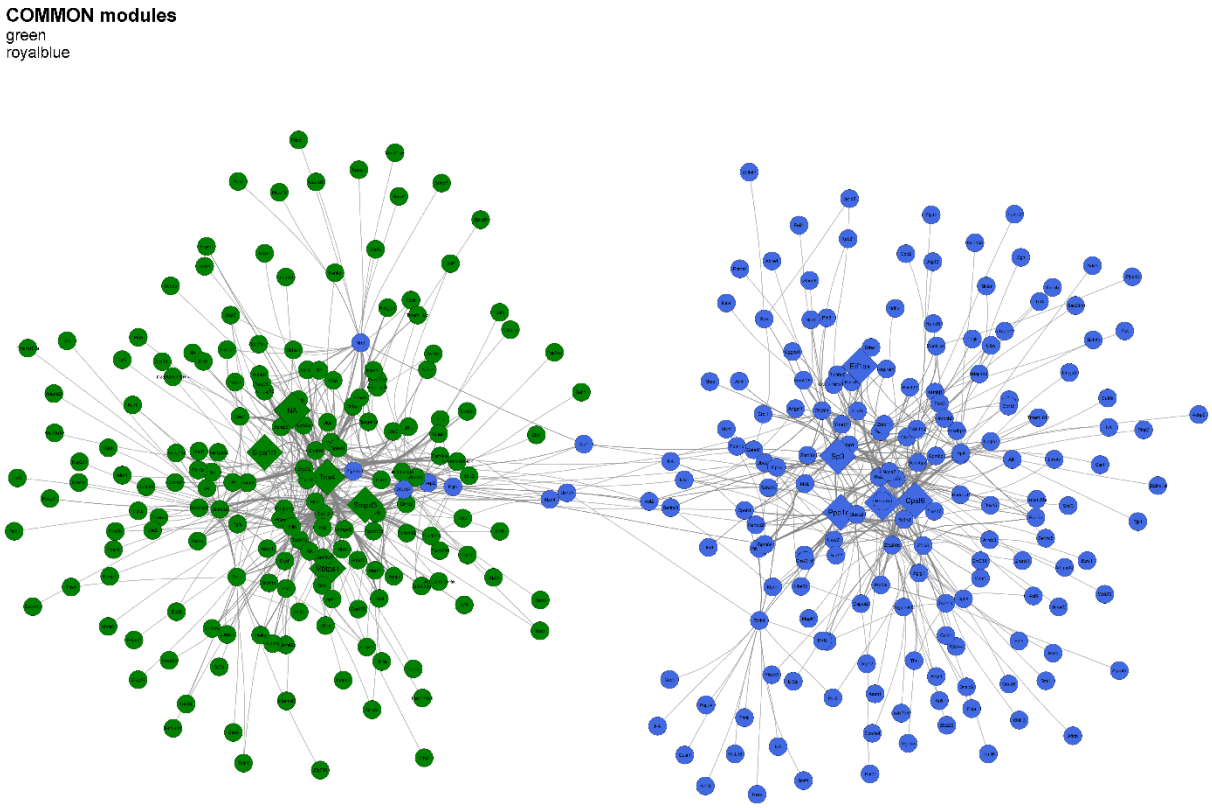

Figure S14. Gene interactions network for the common group of modules green-royalblue. Each node corresponds to a gene, and is colored according to its module. All genes detected as “hub genes” are represented with a diamond shape.

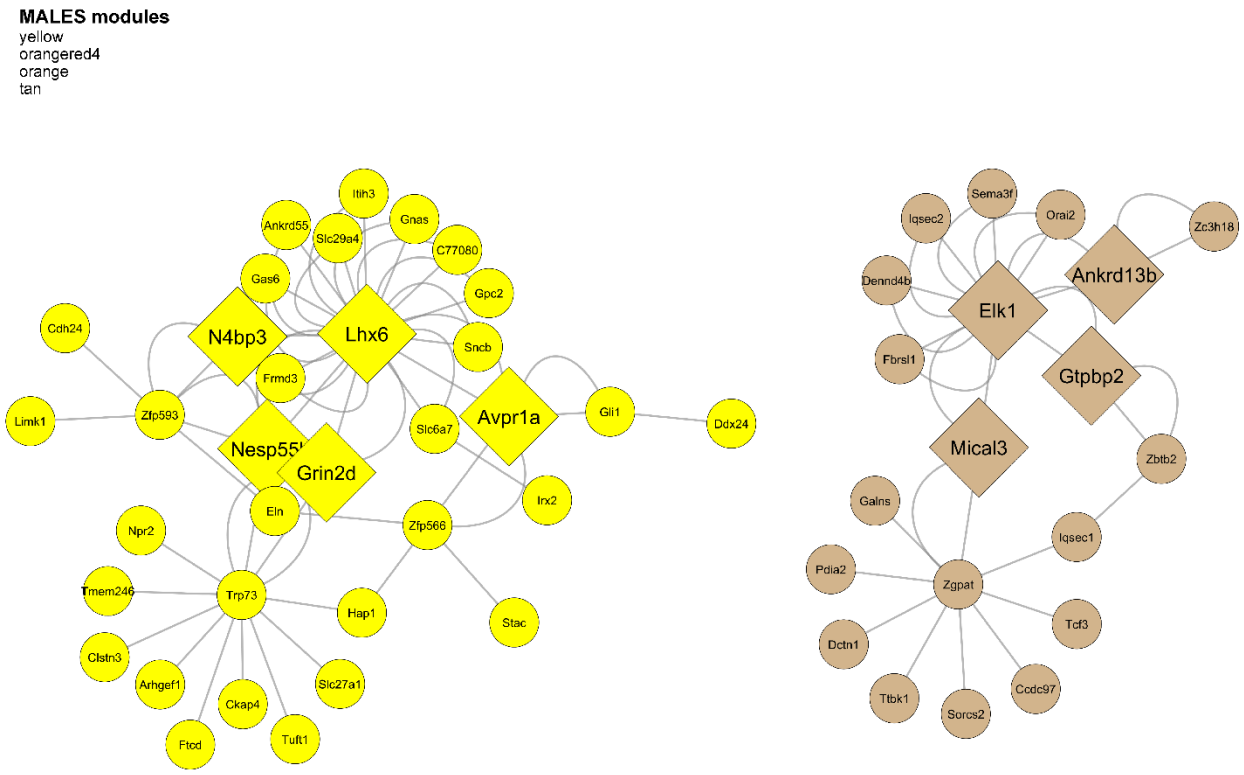

Figure S15. Gene interactions network for the male-specific group of modules yellow-orangered4-orange-tan. Each node corresponds to a gene and is colored according to its module. All genes detected as “hub genes” are represented with a diamond shape.

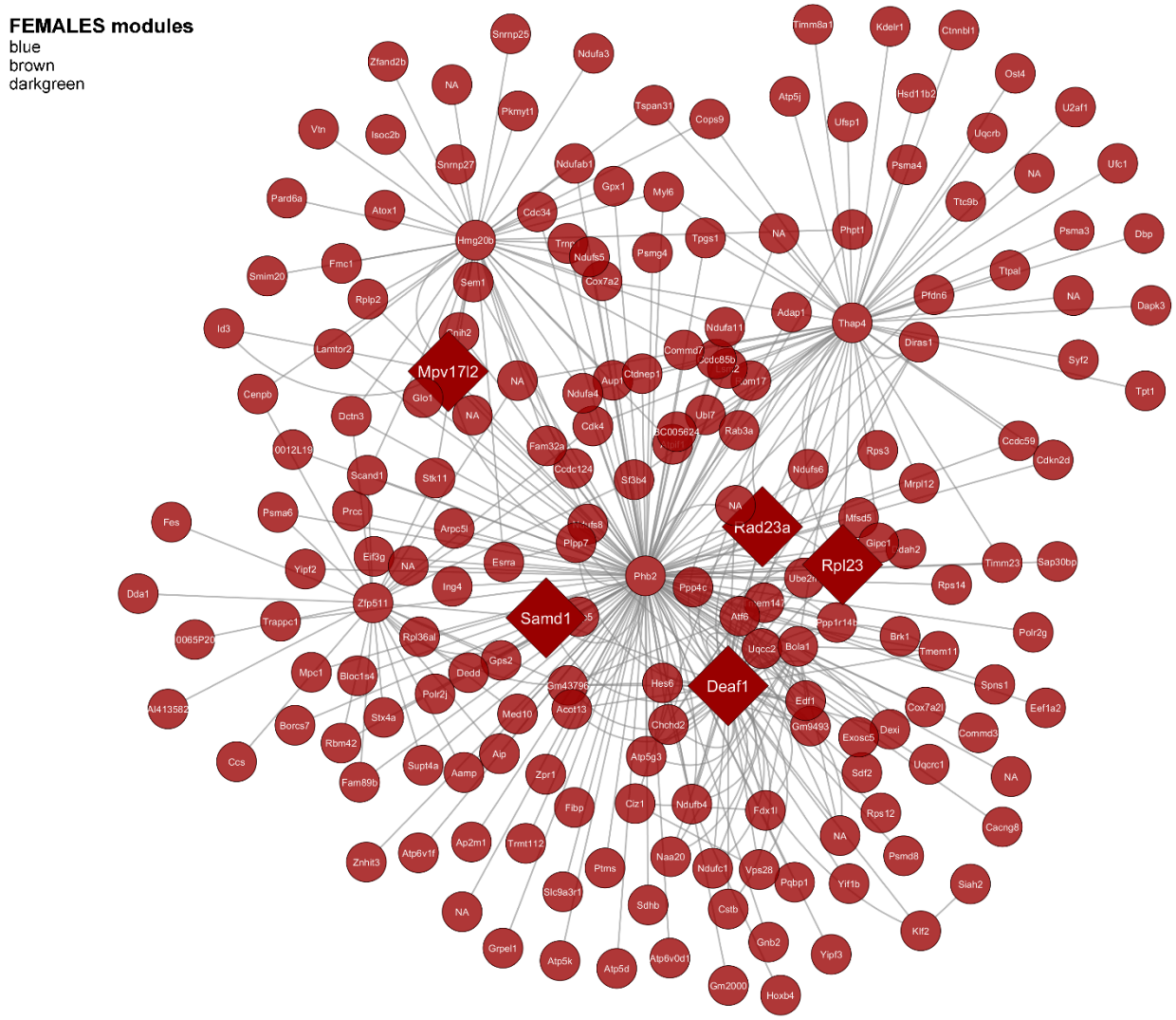

Figure S16. Gene interactions network for the female-specific group of modules blue-brown-darkgreen. Each node corresponds to a gene and is colored according to its module. All genes detected as “hub genes” are represented with a diamond shape.

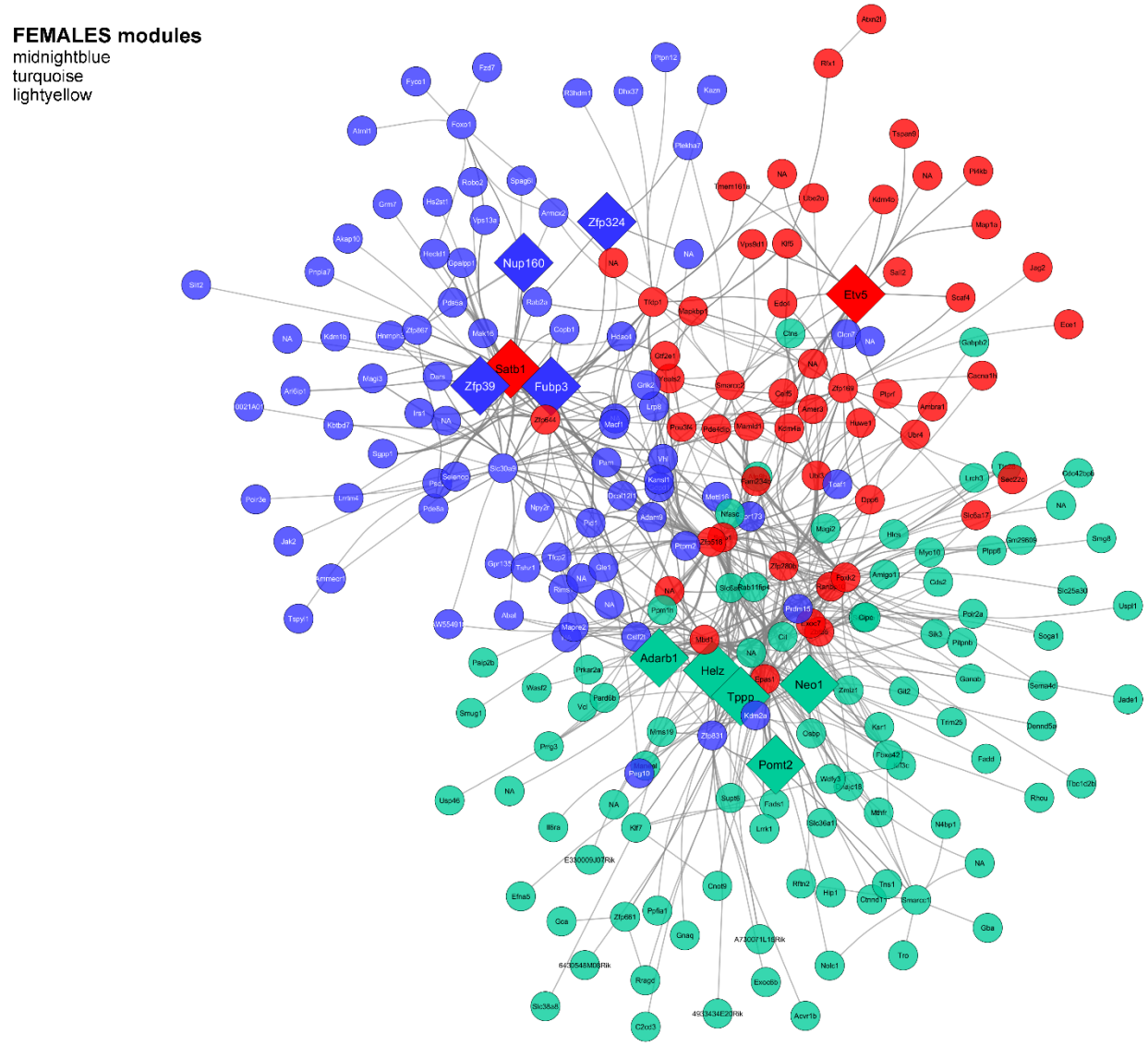

Figure S17. Gene interactions network for the male-specific group of modules midnightblue-turquoise-lightyellow. Each node corresponds to a gene and is colored according to its module. All genes detected as “hub genes” are represented with a diamond shape.

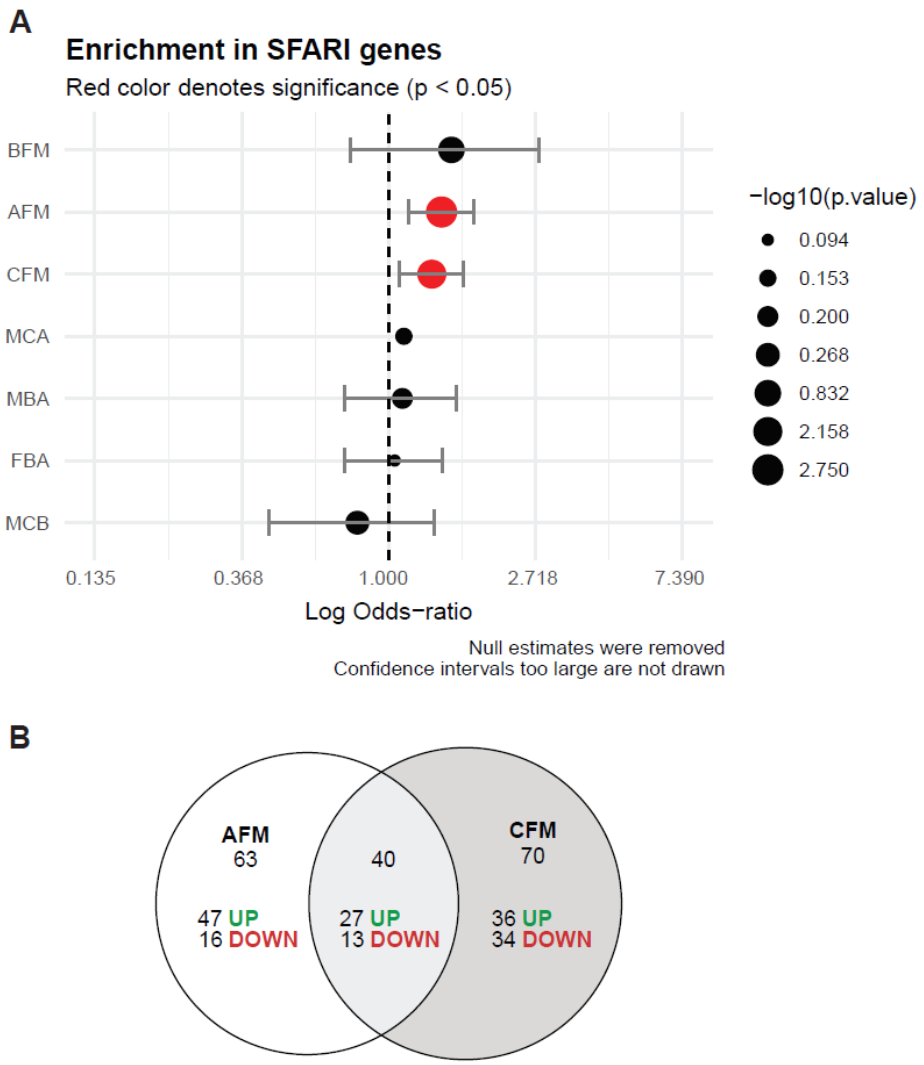

Figure S18. Enrichment in autism spectrum disorders-related genes. (A) The enrichment in genes related to autism spectrum disorders (ASD) from the SFARI Gene database was tested in all sets of differentially expressed genes and depicted as log of the corresponding odd-ratio. Note that null estimates were excluded from the plot, and that significant enrichments ($p < 0.05$) are highlighted in red. (B) Euler diagram depicting the degree of overlap in ASD-related genes between the sexually-biased genes at baseline (AFM) and following 3 weeks of cohabitation with a partner (CFM). The area of each circle is proportional to the number of genes included (detailed within each intersect).

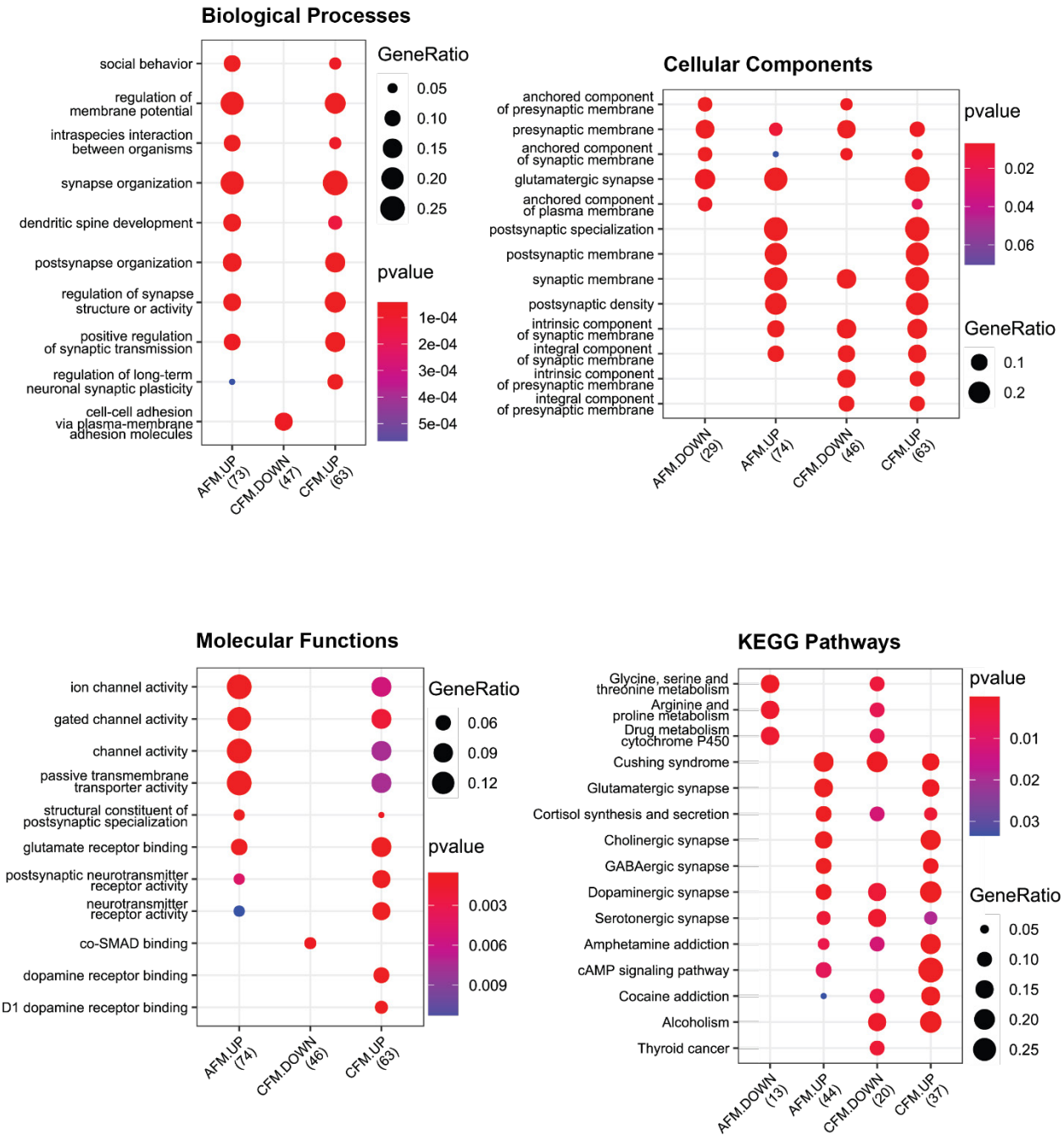

Figure S19. Functional analysis of differentially expressed genes linked to autism spectrum disorder (ASD). Gene ontology enrichments were tested against the biological processes, cellular components, and molecular functions categories, as well as the Kyoto Encyclopedia of Genes and Genomes (KEGG) pathways.

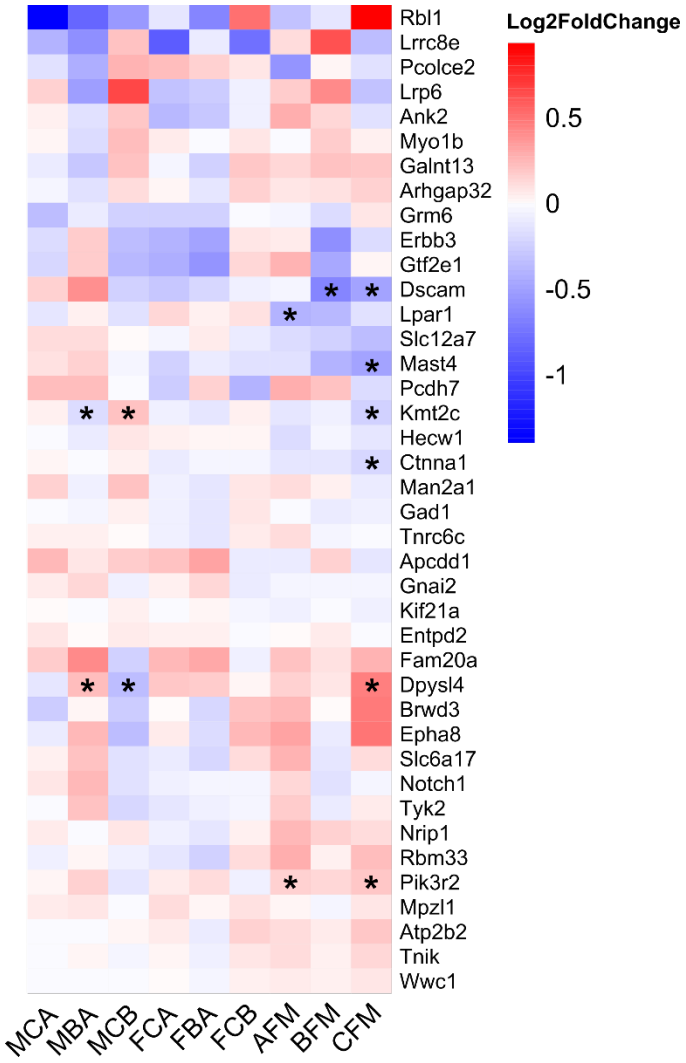

Figure S20. Expression profiles of candidate genes for monogamy. The list of candidate genes was extracted from Young *et al.*, 2019 (REF) and their expression (log2 of fold-change) in each comparison in our dataset is depicted as heatmap. The asterisk symbols depict genes identified as differentially expressed in the given comparison. See Table S3 for definition of experimental groups (columns).

Supplementary Tables

Behavior	term	sumsq	df	statistic	p.value	η^2
aggr_dur	Group	1096.6165031	2	31.8132412	0.0000000	0.2960691
aggr_dur	SEX	32.5222359	1	1.8869636	0.1711806	0.0055004
aggr_dur	Group:SEX	113.2389736	2	3.2851036	0.0395970	0.0235845
aggr_dur	Residuals	3240.2216033	188	NA	NA	NA
aggr_freq	Group	825.9756649	2	39.1308487	0.0000000	0.3513978
aggr_freq	SEX	73.5152471	1	6.9656144	0.0090064	0.0193561
aggr_freq	Group:SEX	70.7450478	2	3.3515682	0.0371348	0.0216634
aggr_freq	Residuals	1984.1561108	188	NA	NA	NA
ano_dur	Group	17.6377312	2	8.5270474	0.0002852	0.0956867
ano_dur	SEX	0.0116866	1	0.0112999	0.9154569	0.0000439
ano_dur	Group:SEX	0.0447143	2	0.0216174	0.9786170	0.0002079
ano_dur	Residuals	194.4338596	188	NA	NA	NA
ano_freq	Group	27.0557825	2	10.5851665	0.0000440	0.1145066
ano_freq	SEX	0.4272880	1	0.3343400	0.5638066	0.0013814
ano_freq	Group:SEX	0.2489760	2	0.0974081	0.9072315	0.0009152
ano_freq	Residuals	240.2648601	188	NA	NA	NA
def_dur	Group	3.3055576	2	1.1133035	0.3306277	0.0194185
def_dur	SEX	11.2127490	1	7.5528516	0.0065753	0.0327257
def_dur	Group:SEX	6.5316628	2	2.1998477	0.1136648	0.0216751
def_dur	Residuals	279.0994634	188	NA	NA	NA
def_freq	Group	14.3615084	2	2.7539800	0.0662441	0.0279206
def_freq	SEX	24.4431473	1	9.3744940	0.0025227	0.0392233
def_freq	Group:SEX	16.7201205	2	3.2062702	0.0427323	0.0307695
def_freq	Residuals	490.1930356	188	NA	NA	NA
explore_dur	Group	13.6524949	2	5.4062426	0.0052136	0.0546930
explore_dur	SEX	0.6420234	1	0.5084688	0.4766866	0.0023164
explore_dur	Group:SEX	0.4562453	2	0.1806683	0.8348570	0.0018090
explore_dur	Residuals	237.3801197	188	NA	NA	NA
explore_freq	Group	29.3743562	2	10.1079000	0.0000677	0.1067175
explore_freq	SEX	3.9973713	1	2.7510410	0.0988586	0.0111031
explore_freq	Group:SEX	2.9292604	2	1.0079769	0.3669202	0.0093594
explore_freq	Residuals	273.1714295	188	NA	NA	NA
nose2nose_dur	Group	40.1066498	2	18.4414445	0.0000000	0.1779147
nose2nose_dur	SEX	2.2867817	1	2.1029709	0.1486795	0.0075996
nose2nose_dur	Group:SEX	3.2088166	2	1.4754464	0.2313123	0.0125868
nose2nose_dur	Residuals	204.4322013	188	NA	NA	NA
nose2nose_freq	Group	37.1555029	2	14.9671743	0.0000009	0.1585131
nose2nose_freq	SEX	0.5300454	1	0.4270313	0.5142477	0.0015163
nose2nose_freq	Group:SEX	2.2661302	2	0.9128544	0.4031484	0.0080787
nose2nose_freq	Residuals	233.3518132	188	NA	NA	NA
rest_dur	Group	12.8886698	2	5.2301605	0.0061590	0.0583214
rest_dur	SEX	0.7926581	1	0.6433137	0.4235261	0.0028407
rest_dur	Group:SEX	0.4268309	2	0.1732060	0.8410984	0.0017267
rest_dur	Residuals	231.6439342	188	NA	NA	NA
rest_freq	Group	20.7392392	2	5.0454661	0.0073378	0.0565293
rest_freq	SEX	0.0233638	1	0.0113679	0.9152038	0.0000391
rest_freq	Group:SEX	0.5201714	2	0.1265479	0.8812069	0.0012684
rest_freq	Residuals	386.3842222	188	NA	NA	NA

Table S1. Statistical analysis of behavioral data. This table details the statistical results for the behavioral data reported in Figure S1. All data were analyzed using two-way ANOVA with Cohabitation and Sex and independent factors.

Sex	Comparison	Code	DE genes	Up	Down
Males	3W vs SN	MCA	39	23 (59%)	16 (41%)
Males	24H vs SN	MBA	529	216 (41%)	313 (59%)
Males	3W vs 24H	MCB	318	209 (66%)	109 (34%)
Females	3W vs SN	FCA	1	1 (100%)	0
Females	24H vs SN	FBA	741	417 (56%)	324 (44%)
Females	3W vs 24H	FCB	18	11 (61%)	7 (39%)
Females vs Males	SN	AFM	1,371	670 (49%)	701 (51%)
Females vs Males	24H	BFM	155	50 (32%)	105 (68%)
Females vs Males	3W	CFM	1,678	863 (51%)	815 (49%)

Table S2. Differential expression analyses summary statistics. Summary statistics for all pairwise comparisons including the number of differentially expressed (DE) genes as well as the direction of fold-change (Up: up-regulated, Down: down-regulated).

Measure	Factor	degrees of freedom	F value	*p*-value	η^2
mtDNA					
Nd1	Cohabitation	2,52	0.73	0.488	0.019
Nd1	Sex	1,52	10.07	0.002	0.131
Nd1	Interaction	2,52	6.57	0.003	0.170
Nd4l	Cohabitation	2,51	4.09	0.022	0.10
Nd4l	Sex	1,51	17.44	0.0001	0.213
Nd4l	Interaction	2,51	1.89	0.162	0.046
mRNA					
Mfn1	Cohabitation	2,44	0.33	0.718	0.013
Mfn1	Sex	1,44	4.88	0.032	0.090
Mfn1	Interaction	2,44	3.07	0.056	0.113
Mfn2	Cohabitation	2,42	0.73	0.486	0.031
Mfn2	Sex	1,42	0.08	0.774	0.002
Mfn2	Interaction	2,42	1.48	0.238	0.063
Fis1	Cohabitation	2,41	0.18	0.838	0.007
Fis1	Sex	1,41	0.14	0.706	0.003
Fis1	Interaction	2,41	3.84	0.029	0.154
Dnm1l	Cohabitation	2,39	4.64	16.000	0.165
Dnm1l	Sex	1,39	2.07	0.158	0.037
Dnm1l	Interaction	2,39	5.01	0.012	0.179

Table S3. Statistical analysis of semi-quantitative real-time PCR data. This table details the statistical results for the molecular data reported in Figure 6. All data were analyzed using two-way ANOVA with Cohabitation and Sex and independent factors.

	24H vs SN	3W vs SN	3W vs 24H	Any
RIT-responsive genes				
Males	13 (2.6%)	3 (9.09%)	8 (2.88%)	20 (3.03%)
Immediate early genes				
Males	3 (0.6%)	2 (6.1%)	4 (1.4%)	7 (1.1%)
Females	7 (1.0%)	0	1 (5.9%)	8 (1.1%)

Table S4. Number of resident-intruder test (RIT)-responsive genes or immediate early genes (IEGs) among differentially expressed genes detected in the nucleus accumbens of male or female prairie voles following cohabitation with a partner. RIT-responsive genes were curated from Supplemental Dataset S6 from Rittschof *et al.*, 2014 (110), and correspond to genes showing differential expression in the mouse ventral hypothalamus 15 min after a 10 min exposure to a conspecific intruder. IEGs were identified from Table S3 of Wu *et al.*, 2017 (111). The percentage of all differentially expressed genes in the given comparison is depicted in parenthesis.

Measure	Factor	degrees of freedom	F value	*p*-value	η^2
Complex I (state 2)	Cohabitation	1,25	0.56	0.460	0.021
Complex I (state 2)	Sex	1,25	0.18	0.676	0.007
Complex I (state 2)	Interaction	1,25	0.46	0.505	0.017
Complex I (state 3)	Cohabitation	1,25	1.53	0.227	0.057
Complex I (state 3)	Sex	1,25	0.11	0.741	0.004
Complex I (state 3)	Interaction	1,25	0.15	0.703	0.005
Complex II	Cohabitation	1,25	0.10	0.758	0.004
Complex II	Sex	1,25	0.02	0.891	0.001
Complex II	Interaction	1,25	2.01	0.168	0.074
Complex I-II junction	Cohabitation	1,25	0.05	0.825	0.002
Complex I-II junction	Sex	1,25	2.07	0.162	0.066
Complex I-II junction	Interaction	1,25	4.34	0.048	0.139
Cytochrome C	Cohabitation	1,25	0.11	0.744	0.004
Cytochrome C	Sex	1,25	1.51	0.230	0.054
Cytochrome C	Interaction	1,25	1.37	0.252	0.049
Complex IV	Cohabitation	1,25	0.43	0.517	0.015
Complex IV	Sex	1,25	< 0.01	0.987	0.000
Complex IV	Interaction	1,25	2.48	0.128	0.089

Table S5. Statistical analysis of respirometry data. This table details the statistical results for the respirometry data reported in Figure S7. All data were analyzed using two-way ANOVA with Cohabitation and Sex and independent factors.

Table S6 can be found as a separate XLSX file.

Table S6. Functional enrichment of sexually-biased genes. This table lists the enriched Biological Processes (BP), Cellular Components (CC), and Molecular Functions (MF) gene ontologies (GO), as well as the enriched pathways from the Kyoto Encyclopedia of Genes and Genomes (KEGG) for the genes sexually-biased in the following groups: only following 3 weeks (3W_only) or 24 hrs (24H_only) of cohabitation, only at baseline (SN_only), or common between baseline and following 3 weeks of cohabitation (3W_SN_intersect).

Gene	GenBank #	Primer sequence (5' - 3')	Amplicon length (bp)
mRNA			
Mfn1	XM_005343764.2	TAATCCAGCAACCCCAGACG TCCAAATCACTCCCCCAACA	122
Mfn2	XM_005353743	CCCTGCTCTTCTCTCGATGC TCCTGTGGGTGTCTTCAAGG	183
Fis1	XM_026784918	ACAGTTTGAGTACGCCTGGT GGGCCTTTTCATACTCCTTGA	170
Dnm1l/Drp1	XM_026777629	ATTCTGCAGCTGGTCCACGT TGTAGCAGGGTTCCAGTTCTGA	90
Hprt1	XM_005358462.1	TCCCAGCGTCGTGATTAGTG TCGAGCCAGTCTTTCAGTCC	139
gDNA			
Nd1	NC_027945.1	AGAACCCCTACGTCCCCTAG TGGGTGAGGCATGGGTATTG	109
Nd4l	NC_027945.1	ATCCTAGTCTTTGCCGCCTG AGTCAGAGCCGTAAGTGTTTGA	79
Gapdh	NW_004949099.1	TCAACCAGTCCCAGCACAAG GGGTTGGGAGGAAACGAGAG	92

Table S7. Description of all the PCR primers used in this study.

Table S8 can be found as a separate XLSX file.

Table S8. List of genes with at least one differential transcript usage. For each pairwise comparison, this table lists each gene with at least one differentially expressed transcript.

Category	Group of modules	Hub gene	Differential expression	Functional evidence of interest	Reference (PMID)
Common	green-royalblue	Eif1ax	MBA ↓, AFM ↓	Translation initiation	24499181
Common	green-royalblue	Cpsf6	MBA ↓, MCB ↑, AFM ↓	Component of the cleavage factor Im complex responsible for pre-mRNA cleavage and polyadenylation processing	9659921
Common	green-royalblue	Sp3	MBA ↓, MCB ↑	Transcription factor regulating synaptic function and plasticity	28793257
Common	green-royalblue	Fnip1	MBA ↓, AFM ↓	Regulates mTOR signaling	22608497
Common	green-royalblue	Fnip1	MBA ↓, AFM ↓	Regulates mitochondrion organization	25775561
Common	green-royalblue	Smpd3	AFM ↑	Regulates the Golgi secretory pathway	27882938
Common	green-royalblue	Smpd3	AFM ↑	SMPD3 deficiency perturbs neuronal proteostasis and causes progressive cognitive impairment	29725009
Common	green-royalblue	Smpd3	AFM ↑	Regulates dopamine transporter trafficking	29329781
Common	green-royalblue	Mbtps1	CFM ↑	regulates mega vesicle-mediated collagen trafficking	30046013
Common	green-royalblue	Tox4	AFM ↑, CFM ↑	Regulates chromatin structure	20516061
Common	green-royalblue	Abcc5	FBA ↓, AFM ↑	Cyclic nucleotides transporter involved in cellular export of endogenous metabolites	26515061
Common	green-royalblue	Sipa1l1	AFM ↑	Required for synaptic plasticity underlying learning and memory	19442707
Common	cyan-saddlebrown	Asna1	FBA ↑	Controls endoplasmic reticulum homeostasis	26438609
Common	cyan-saddlebrown	Gtpbp3	MBA ↑, AFM ↑	Mitochondrial GTP-binding protein involved in tRNA modification	14680828
Common	cyan-saddlebrown	Rnf126	FBA ↑	Ubiquitin E3 ligase regulating EGFR sorting	23418353
Common	cyan-saddlebrown	Tspan4	FBA ↑	Integrins and antigen binding	9360996
Males	yellow-tan	Ankrd13b	MBA ↑, AFM ↑	Ubiquitin-binding protein regulating the internalization of ligand-activated EGFR	22298428
Females	brown	Rad23a	FBA ↑	Involved in delivery of poly-ubiquitinated proteins to the proteasome	26998601
Females	midnightblue-turquoise-red	Satb1	FBA ↓	Recruits histone deacetylases to repress interleukin-2 receptor alpha	12374985
Females	midnightblue-turquoise-red	Fubp3	FBA ↓	RNA-binding protein that regulates dendritic targeting of MAP2 mRNAs	23121659
Females	midnightblue-turquoise-red	Adarb1	FBA ↓, AFM ↑	RNA editing of serotonin and glutamate receptors; in the nucleus accumbens, involved in ethanol preference after chronic alcohol exposition	30697154
Females	midnightblue-turquoise-red	Neo1	FBA ↓	Regulates mitochondrial activity	27913301
Females	midnightblue-turquoise-red	Neo1	FBA ↓	Regulates EPSP frequency in the amygdala and fear memory impairments	30228230
Females	midnightblue-turquoise-red	Neo1	FBA ↓	Promotes acute inflammation	22412855

Table S9. Functional annotation of differentially expressed candidate hub genes. This table lists all candidate hub genes showing differential expression in any pairwise comparison and provides relevant functional evidence from the literature. PMID: PubMed ID.

Table S10 can be found as a separate XLSX file.

Table S10. Differential expression analysis in the prairie vole nucleus accumbens following cohabitation with an opposite-sex partner. For each gene, this table lists the differential expression analysis results as outputted by DESeq2 for each pairwise comparison. All columns with their name starting with “DE.” encode the differentially expressed (DE) status (0: not differentially expressed, 1: differentially expressed) for convenience, defined as adjusted *p*-value < 0.1.

Table S11 can be found as a separate XLSX file.

Table S11. Autism spectrum disorders-related genes differentially expressed in the prairie vole nucleus accumbens following cohabitation. This table lists all genes from the SFARI Gene database detected in our study alongside their differential expression results as outputted by DESeq2. All columns with their name starting with “DE.” encode the differentially expressed (DE) status (0: not differentially expressed, 1: differentially expressed) for convenience, defined as adjusted *p*-value < 0.1.

Table S12 can be found as a separate XLSX file.

Table S12. Functional enrichment of differentially expressed genes. This table lists the enriched Biological Processes (BP), Cellular Components (CC), and Molecular Functions (MF) gene ontologies (GO), as well as the enriched pathways from the Kyoto Encyclopedia of Genes and Genomes (KEGG) for differentially expressed genes in each pairwise comparison. For each functional enrichment category, the enrichment results are presented when accounting for the gene’s directionality of regulation (UP- or DOWN-regulated) or not on two separate sheets. See Table S2 for experimental group codes.

Table S13 can be found as a separate XLSX file.

Table S13 Functional enrichment of differentially expressed genes linked to autism spectrum disorder (ASD). This table lists the enriched Biological Processes (BP), Cellular Components (CC), and Molecular Functions (MF) gene ontologies (GO), as well as the enriched pathways from the Kyoto Encyclopedia of Genes and Genomes (KEGG) for the genes from the SFARI Gene database linked to ASD (syndromic) and differentially expressed genes in our dataset. For each functional enrichment category, the enrichment results are presented when accounting for the gene's directionality of regulation (UP- or DOWN-regulated) or not on two separate sheets. See Table S2 for experimental group codes.

Supplementary References

1. Young KA, Gobrogge KL, Liu Y, Wang Z (2011): The neurobiology of pair bonding: insights from a socially monogamous rodent. *Front Neuroendocrinol* 32: 53–69.

2. Duclot F, Kabbaj M (2015): The estrous cycle surpasses sex differences in regulating the transcriptome in the rat medial prefrontal cortex and reveals an underlying role of early growth response 1. *Genome Biol* 16: 256.

3. Resendez SL, Kuhnmuench M, Krzywosinski T, Aragona BJ (2012): κ-Opioid receptors within the nucleus accumbens shell mediate pair bond maintenance. *J Neurosci* 32: 6771–6784.

4. Shannon P, Markiel A, Ozier O, Baliga NS, Wang JT, Ramage D, *et al.* (2003): Cytoscape: a software environment for integrated models of biomolecular interaction networks. *Genome Res* 13: 2498–2504.

5. Resendez SL, Keyes PC, Day JJ, Hambro C, Austin CJ, Maina FK, *et al.* (2016): Dopamine and opioid systems interact within the nucleus accumbens to maintain monogamous pair bonds. *Elife* 5. https://doi.org/10.7554/eLife.15325

6. Bales KL, Plotsky PM, Young LJ, Lim MM, Grotte N, Ferrer E, Carter CS (2007): Neonatal oxytocin manipulations have long-lasting, sexually dimorphic effects on vasopressin receptors. *Neuroscience* 144: 38–45.

7. Aragona BJ, Liu Y, Yu YJ, Curtis JT, Detwiler JM, Insel TR, Wang Z (2006): Nucleus accumbens dopamine differentially mediates the formation and maintenance of monogamous pair bonds. *Nat Neurosci* 9: 133–139.

8. King LB, Walum H, Inoue K, Eyrich NW, Young LJ (2016): Variation in the Oxytocin Receptor Gene Predicts Brain Region-Specific Expression and Social Attachment. *Biol Psychiatry* 80: 160–169.

9. Duclot F, Wang H, Youssef C, Liu Y, Wang Z, Kabbaj M (2016): Trichostatin A (TSA) facilitates formation of partner preference in male prairie voles (Microtus ochrogaster). *Horm Behav* 81: 68–73.

10. Hammock EAD, Young LJ (2005): Microsatellite instability generates diversity in brain and sociobehavioral traits. *Science* 308: 1630–1634.

11. Wang H, Duclot F, Liu Y, Wang Z, Kabbaj M (2013): Histone deacetylase inhibitors facilitate partner preference formation in female prairie voles. *Nat Neurosci* 16: 919–924.

12. Barrett CE, Keebaugh AC, Ahern TH, Bass CE, Terwilliger EF, Young LJ (2013): Variation in vasopressin receptor (Avpr1a) expression creates diversity in behaviors related to monogamy in prairie voles. *Horm Behav* 63: 518–526.

13. Gobrogge KL, Liu Y, Jia X, Wang Z (2007): Anterior hypothalamic neural activation and neurochemical associations with aggression in pair-bonded male prairie voles. *J Comp Neurol* 502: 1109–1122.

14. Okhovat M, Berrio A, Wallace G, Ophir AG, Phelps SM (2015): Sexual fidelity trade-offs promote regulatory variation in the prairie vole brain. *Science* 350: 1371–1374.

15. Blumstein DT, Daniel JC, Evans CS (2010): JWatcher Software. Retrieved from http://www.jwatcher.ucla.edu/

16. Okhovat M, Maguire SM, Phelps SM (2017): Methylation of avpr1a in the cortex of wild prairie voles: effects of CpG position and polymorphism. *R Soc Open Sci* 4: 160646.

17. Edgar R, Domrachev M, Lash AE (2002): Gene Expression Omnibus: NCBI gene expression and hybridization array data repository. *Nucleic Acids Res* 30: 207–210.

18. Williams JR, Catania KC, Carter CS (1992): Development of partner preferences in female prairie voles (Microtus ochrogaster): the role of social and sexual experience. *Horm Behav* 26: 339–349.

19. Chen S, Zhou Y, Chen Y, Gu J (2018): fastp: an ultra-fast all-in-one FASTQ preprocessor. *Bioinformatics* 34: i884–i890.

20. Winslow JT, Hastings N, Carter CS, Harbaugh CR, Insel TR (1993): A role for central vasopressin in pair bonding in monogamous prairie voles. *Nature* 365: 545–548.

21. Andrews S (2014): FastQC. A quality control tool for high throughput sequence data. Babraham Bioinformatics. *FastQC*. Retrieved from http://www.bioinformatics.babraham.ac.uk/projects/fastqc/

22. Dumais KM, Veenema AH (2015): Vasopressin and oxytocin receptor systems in the brain: Sex differences and sex-specific regulation of social behavior. *Front Neuroendocrinol*. https://doi.org/10.1016/j.yfrne.2015.04.003

23. Patro R, Duggal G, Love MI, Irizarry RA, Kingsford C (2017): Salmon provides fast and bias-aware quantification of transcript expression. *Nat Methods* 14: 417–419.

24. Williams AV, Duque-Wilckens N, Ramos-Maciel S, Campi KL, Bhela SK, Xu CK, *et al.* (2020): Social approach and social vigilance are differentially regulated by oxytocin receptors in the nucleus accumbens. *Neuropsychopharmacology*. https://doi.org/10.1038/s41386-020-0657-4

25. Soneson C, Love MI, Robinson MD (2015): Differential analyses for RNA-seq: transcript-level estimates improve gene-level inferences. *F1000Res* 4: 1521.

26. Yao W-D, Gainetdinov RR, Arbuckle MI, Sotnikova TD, Cyr M, Beaulieu J-M, *et al.* (2004): Identification of PSD-95 as a regulator of dopamine-mediated synaptic and behavioral plasticity. *Neuron* 41: 625–638.

27. Love MI, Huber W, Anders S (2014): Moderated estimation of fold change and dispersion for RNA-seq data with DESeq2. *Genome Biol* 15: 550.

28. Zhang J, Vinuela A, Neely MH, Hallett PJ, Grant SGN, Miller GM, *et al.* (2007): Inhibition of the dopamine D1 receptor signaling by PSD-95. *J Biol Chem* 282: 15778–15789.

29. Huber W, Carey VJ, Gentleman R, Anders S, Carlson M, Carvalho BS, *et al.* (2015): Orchestrating high-throughput genomic analysis with Bioconductor. *Nat Methods* 12: 115–121.

30. Morigaki R, Goto S (2015): Postsynaptic density protein 95 in the striosome and matrix compartments of the human neostriatum. *Front Neuroanat* 9: 154.

31. Subramanian A, Tamayo P, Mootha VK, Mukherjee S, Ebert BL, Gillette MA, *et al.* (2005): Gene set enrichment analysis: a knowledge-based approach for interpreting genome-wide expression profiles. *Proc Natl Acad Sci U S A* 102: 15545–15550.

32. Sun P, Wang J, Gu W, Cheng W, Jin G-Z, Friedman E, *et al.* (2009): PSD-95 regulates D1 dopamine receptor resensitization, but not receptor-mediated Gs-protein activation. *Cell Res* 19: 612–624.

33. Fiorentini C, Mattanza C, Collo G, Savoia P, Spano P, Missale C (2011): The tyrosine phosphatase Shp-2 interacts with the dopamine D(1) receptor and triggers D(1) -mediated Erk signaling in striatal neurons. *J Neurochem* 117: 253–263.

34. Scheggi S, De Montis MG, Gambarana C (2018): DARPP-32 in the orchestration of responses to positive natural stimuli. *J Neurochem* 147: 439–453.

35. Merico D, Isserlin R, Stueker O, Emili A, Bader GD (2010): Enrichment map: a network-based method for gene-set enrichment visualization and interpretation. *PLoS One* 5: e13984.

36. Young RL, Ferkin MH, Ockendon-Powell NF, Orr VN, Phelps SM, Pogány Á, *et al.* (2019): Conserved transcriptomic profiles underpin monogamy across vertebrates. *Proc Natl Acad Sci U S A* 116: 1331–1336.

37. Reimand J, Isserlin R, Voisin V, Kucera M, Tannus-Lopes C, Rostamianfar A, *et al.* (2019): Pathway enrichment analysis and visualization of omics data using g:Profiler, GSEA, Cytoscape and EnrichmentMap. *Nat Protoc* 14: 482–517.

38. Smedley D, Haider S, Ballester B, Holland R, London D, Thorisson G, Kasprzyk A (2009): BioMart--biological queries made easy. *BMC Genomics* 10: 22.

39. Davis AP, Grondin CJ, Johnson RJ, Sciaky D, McMorran R, Wiegers J, *et al.* (2019): The Comparative Toxicogenomics Database: update 2019. *Nucleic Acids Res* 47: D948–D954.

40. R Core Team (2020): R: A language and environment for statistical computing. R Foundation for Statistical Computing. Vienna, Austria. Retrieved from https://www.R-project.org/

41. Abrahams BS, Arking DE, Campbell DB, Mefford HC, Morrow EM, Weiss LA, *et al.* (2013): SFARI Gene 2.0: a community-driven knowledgebase for the autism spectrum disorders (ASDs). *Mol Autism* 4: 36.

42. SFARI Gene (n.d.): *SFARI Gene*. Retrieved April 22, 2020, from https://gene.sfari.org/

43. Yu G, Wang L-G, Han Y, He Q-Y (2012): clusterProfiler: an R package for comparing biological themes among gene clusters. *OMICS* 16: 284–287.

44. Love MI, Soneson C, Patro R (2018): Swimming downstream: statistical analysis of differential transcript usage following Salmon quantification. *F1000Res* 7: 952.

45. Nowicka M, Robinson MD (2016): DRIMSeq: a Dirichlet-multinomial framework for multivariate count outcomes in genomics. *F1000Res* 5: 1356.

46. Van den Berge K, Clement L (2019): stageR: stageR: stage-wise analysis of high throughput gene expression data in R.

47. Zhang B, Horvath S (2005): A general framework for weighted gene co-expression network analysis. *Stat Appl Genet Mol Biol* 4: Article17.

48. Langfelder P, Horvath S (2008): WGCNA: an R package for weighted correlation network analysis. *BMC Bioinformatics* 9: 559.

49. Langfelder P, Horvath S (2012): Fast R Functions for Robust Correlations and Hierarchical Clustering. *J Stat Softw* 46. Retrieved from https://www.ncbi.nlm.nih.gov/pubmed/23050260

50. Lachmann A, Giorgi FM, Lopez G, Califano A (2016): ARACNe-AP: gene network reverse engineering through adaptive partitioning inference of mutual information. *Bioinformatics* 32: 2233–2235.

51. Schmeier S, Alam T, Essack M, Bajic VB (2017): TcoF-DB v2: update of the database of human and mouse transcription co-factors and transcription factor interactions. *Nucleic Acids Res* 45: D145–D150.

52. Bagot RC, Cates HM, Purushothaman I, Lorsch ZS, Walker DM, Wang J, *et al.* (2016): Circuit-wide Transcriptional Profiling Reveals Brain Region-Specific Gene Networks Regulating Depression Susceptibility. *Neuron* 90: 969–983.

53. Zhang B, Gaiteri C, Bodea L-G, Wang Z, McElwee J, Podtelezhnikov AA, *et al.* (2013): Integrated systems approach identifies genetic nodes and networks in late-onset Alzheimer's disease. *Cell* 153: 707–720.

54. Shu L, Zhao Y, Kurt Z, Byars SG, Tukiainen T, Kettunen J, *et al.* (2016): Mergeomics: multidimensional data integration to identify pathogenic perturbations to biological systems. *BMC Genomics* 17: 874.

55. Hollis F, Duclot F, Gunjan A, Kabbaj M (2011): Individual differences in the effect of social defeat on anhedonia and histone acetylation in the rat hippocampus. *Horm Behav* 59: 331–337.

56. Gnaiger E (2008): Polarographic oxygen sensors, the oxygraph and high-resolution respirometry to assess mitochondrial function. *Drug-induced mitochondrial dysfunction* 327: 352.

57. Herbst EAF, Holloway GP (2015): Permeabilization of brain tissue in situ enables multiregion analysis of mitochondrial function in a single mouse brain. *J Physiol* 593: 787–801.

58. Laouafa S, Roussel D, Marcouiller F, Soliz J, Gozal D, Bairam A, Joseph V (2019): Roles of oestradiol receptor alpha and beta against hypertension and brain mitochondrial dysfunction under intermittent hypoxia in female rats. *Acta Physiol* 226: e13255.

59. Carter CS, Witt DM, Auksi T, Casten L (1987): Estrogen and the induction of lordosis in female and male prairie voles (Microtus ochrogaster). *Horm Behav* 21: 65–73.

60. Cohen-Parsons M, Carter CS (1987): Males increase serum estrogen and estrogen receptor binding in brain of female voles. *Physiol Behav* 39: 309–314.

61. Carter CS, Witt DM, Schneider J, Harris ZL, Volkening D (1987): Male stimuli are necessary for female sexual behavior and uterine growth in prairie voles (Microtus ochrogaster). *Horm Behav* 21: 74–82.

62. Carter CS, Witt DM, Manock SR, Adams KA, Bahr JM, Carlstead K (1989): Hormonal correlates of sexual behavior and ovulation in male-induced and postpartum estrus in female prairie voles. *Physiol Behav* 46: 941–948.

63. Carter CS, Getz LL, Gavish L, McDermott JL, Arnold P (1980): Male-related pheromones and the activation of female reproduction in the prairie vole (Microtus ochrogaster). *Biol Reprod* 23: 1038–1045.

64. Carter CS, DeVries AC, Getz LL (1995): Physiological substrates of mammalian monogamy: the prairie vole model. *Neurosci Biobehav Rev* 19: 303–314.

65. Lei K, Cushing BS, Musatov S, Ogawa S, Kramer KM (2010): Estrogen Receptor-α in the Bed Nucleus of the Stria Terminalis Regulates Social Affiliation in Male Prairie Voles (Microtus ochrogaster). *PLoS ONE* 5: e8931.

66. Cushing BS, Razzoli M, Murphy AZ, Epperson PM, Le W-W, Hoffman GE (2004): Intraspecific variation in estrogen receptor alpha and the expression of male sociosexual behavior in two populations of prairie voles. *Brain Res* 1016: 247–254.

67. Yang X, Schadt EE, Wang S, Wang H, Arnold AP, Ingram-Drake L, *et al.* (2006): Tissue-specific expression and regulation of sexually dimorphic genes in mice. *Genome Res* 16: 995–1004.

68. Xu H, Wang F, Liu Y, Yu Y, Gelernter J, Zhang H (2014): Sex-biased methylome and transcriptome in human prefrontal cortex. *Hum Mol Genet* 23: 1260–1270.

69. Guevara R, Gianotti M, Roca P, Oliver J (2011): Age and sex-related changes in rat brain mitochondrial function. *Cell Physiol Biochem* 27: 201–206.

70. Trabzuni D, Ramasamy A, Imran S, Walker R, Smith C, Weale ME, *et al.* (2013): Widespread sex differences in gene expression and splicing in the adult human brain. *Nat Commun* 4: 2771.

71. LaRese TP, Rheaume BA, Abraham R, Eipper BA, Mains RE (2019): Sex-Specific Gene Expression in the Mouse Nucleus Accumbens Before and After Cocaine Exposure. *J Endocr Soc* 3: 468–487.

72. Shi L, Zhang Z, Su B (2016): Sex Biased Gene Expression Profiling of Human Brains at Major Developmental Stages. *Sci Rep* 6: 21181.

73. Krentzel AA, Meitzen J (2018): Biological Sex, Estradiol and Striatal Medium Spiny Neuron Physiology: A Mini-Review. *Front Cell Neurosci* 12: 492.

74. Willett JA, Will T, Hauser CA, Dorris DM, Cao J, Meitzen J (2016): No Evidence for Sex Differences in the Electrophysiological Properties and Excitatory Synaptic Input onto Nucleus Accumbens Shell Medium Spiny Neurons. *eNeuro* 3. https://doi.org/10.1523/ENEURO.0147-15.2016

75. Cao J, Willett JA, Dorris DM, Meitzen J (2018): Sex Differences in Medium Spiny Neuron Excitability and Glutamatergic Synaptic Input: Heterogeneity Across Striatal Regions and Evidence for Estradiol-Dependent Sexual Differentiation. *Front Endocrinol* 9: 173.

76. Proaño SB, Morris HJ, Kunz LM, Dorris DM, Meitzen J (2018): Estrous cycle-induced sex differences in medium spiny neuron excitatory synaptic transmission and intrinsic excitability in adult rat nucleus accumbens core. *J Neurophysiol* 120: 1356–1373.

77. Johnson MB, Kawasawa YI, Mason CE, Krsnik Z, Coppola G, Bogdanović D, *et al.* (2009): Functional and evolutionary insights into human brain development through global transcriptome analysis. *Neuron* 62: 494–509.

78. Piechota M, Korostynski M, Solecki W, Gieryk A, Slezak M, Bilecki W, *et al.* (2010): The dissection of transcriptional modules regulated by various drugs of abuse in the mouse striatum. *Genome Biol* 11: R48.

79. Sun W-L, Zhou L, Hazim R, Quinones-Jenab V, Jenab S (2008): Effects of dopamine and NMDA receptors on cocaine-induced Fos expression in the striatum of Fischer rats. *Brain Res* 1243: 1–9.

80. Cadet JL, Brannock C, Ladenheim B, McCoy MT, Krasnova IN, Lehrmann E, *et al.* (2014): Enhanced upregulation of CRH mRNA expression in the nucleus accumbens of male rats after a second injection of methamphetamine given thirty days later. *PLoS One* 9: e84665.

81. Marie-Claire C, Benturquia N, Lundqvist A, Courtin C, Noble F (2008): Characteristics of dual specificity phosphatases mRNA regulation by 3,4-methylenedioxymethamphetamine acute treatment in mice striatum. *Brain Res* 1239: 42–48.

82. Bell RL, Kimpel MW, McClintick JN, Strother WN, Carr LG, Liang T, *et al.* (2009): Gene expression changes in the nucleus accumbens of alcohol-preferring rats following chronic ethanol consumption. *Pharmacol Biochem Behav* 94: 131–147.

83. Li Y, Xia B, Li R, Yin D, Liang W (2017): Changes in Expression of Dopamine, Its Receptor, and Transporter in Nucleus Accumbens of Heroin-Addicted Rats with Brain-Derived Neurotrophic Factor (BDNF) Overexpression. *Med Sci Monit* 23: 2805–2815.

84. Binder EB, Kinkead B, Owens MJ, Nemeroff CB (2001): Neurotensin and dopamine interactions. *Pharmacol Rev* 53: 453–486.

85. Torruella-Suárez ML, McElligott ZA (2020): Neurotensin in reward processes. *Neuropharmacology* 167: 108005.

86. McHenry JA, Otis JM, Rossi MA, Robinson JE, Kosyk O, Miller NW, *et al.* (2017): Hormonal gain control of a medial preoptic area social reward circuit. *Nat Neurosci* 20: 449–458.

87. Amadei EA, Johnson ZV, Jun Kwon Y, Shpiner AC, Saravanan V, Mays WD, *et al.* (2017): Dynamic corticostriatal activity biases social bonding in monogamous female prairie voles. *Nature* 546: 297–301.

88. Scribner JL, Vance EA, Protter DSW, Sheeran WM, Saslow E, Cameron RT, *et al.* (2020): A neuronal signature for monogamous reunion. *Proc Natl Acad Sci U S A*. https://doi.org/10.1073/pnas.1917287117

89. Massaly N, Dahan L, Baudonnat M, Hovnanian C, Rekik K, Solinas M, *et al.* (2013): Involvement of protein degradation by the ubiquitin proteasome system in opiate addictive behaviors. *Neuropsychopharmacology* 38: 596–604.

90. Caputi FF, Rullo L, Stamatakos S, Candeletti S, Romualdi P (2019): Interplay between the Endogenous Opioid System and Proteasome Complex: Beyond Signaling. *Int J Mol Sci* 20. https://doi.org/10.3390/ijms20061441

91. Werner CT, Mitra S, Martin JA, Stewart AF, Lepack AE, Ramakrishnan A, *et al.* (2019): Ubiquitin-proteasomal regulation of chromatin remodeler INO80 in the nucleus accumbens mediates persistent cocaine craving. *Sci Adv* 5: eaay0351.

92. Werner CT, Viswanathan R, Martin JA, Gobira PH, Mitra S, Thomas SA, *et al.* (2018): E3 Ubiquitin-Protein Ligase SMURF1 in the Nucleus Accumbens Mediates Cocaine Seeking. *Biol Psychiatry* 84: 881–892.

93. Gonzales FR, Howell KK, Dozier LE, Anagnostaras SG, Patrick GN (2018): Proteasome phosphorylation regulates cocaine-induced sensitization. *Mol Cell Neurosci* 88: 62–69.

94. Guang S, Pang N, Deng X, Yang L, He F, Wu L, *et al.* (2018): Synaptopathology Involved in Autism Spectrum Disorder. *Front Cell Neurosci* 12: 470.

95. Bora E, Yucel M, Allen NB (2009): Neurobiology of human affiliative behaviour: implications for psychiatric disorders. *Curr Opin Psychiatry* 22: 320–325.

96. Bourgeron T (2015): From the genetic architecture to synaptic plasticity in autism spectrum disorder. *Nat Rev Neurosci* 16: 551–563.

97. Ueoka I, Pham HTN, Matsumoto K, Yamaguchi M (2019): Autism Spectrum Disorder-Related Syndromes: Modeling with Drosophila and Rodents. *Int J Mol Sci* 20. https://doi.org/10.3390/ijms20174071

98. Santini E, Huynh TN, MacAskill AF, Carter AG, Pierre P, Ruggero D, *et al.* (2013): Exaggerated translation causes synaptic and behavioural aberrations associated with autism. *Nature* 493: 411–415.

99. Chen Y-C, Chang Y-W, Huang Y-S (2019): Dysregulated Translation in Neurodevelopmental Disorders: An Overview of Autism-Risk Genes Involved in Translation. *Dev Neurobiol* 79: 60–74.

100. Holloszy JO, Oscai LB, Don IJ, Molé PA (1970): Mitochondrial citric acid cycle and related enzymes: adaptive response to exercise. *Biochem Biophys Res Commun* 40: 1368–1373.

101. Williams RS, Salmons S, Newsholme EA, Kaufman RE, Mellor J (1986): Regulation of nuclear and mitochondrial gene expression by contractile activity in skeletal muscle. *J Biol Chem* 261: 376–380.

102. Hood DA, Radovan ZAK, Pette D (1989): Chronic stimulation of rat skeletal muscle induces coordinate increases in mitochondrial and nuclear mRNAs of cytochrome-c-oxidase subunits. *European Journal of Biochemistry* 179: 275–280.

103. Hollis F, van der Kooij MA, Zanoletti O, Lozano L, Cantó C, Sandi C (2015): Mitochondrial function in the brain links anxiety with social subordination. *Proc Natl Acad Sci U S A* 112: 15486–15491.

104. van der Kooij MA, Hollis F, Lozano L, Zalachoras I, Abad S, Zanoletti O, *et al.* (2018): Diazepam actions in the VTA enhance social dominance and mitochondrial function in the nucleus accumbens by activation of dopamine D1 receptors. *Mol Psychiatry* 23: 569–578.

105. Gingrich B, Liu Y, Cascio C, Wang Z, Insel TR (2000): Dopamine D2 receptors in the nucleus accumbens are important for social attachment in female prairie voles (Microtus ochrogaster). *Behav Neurosci* 114: 173–183.

106. Quach TT, Wilson SM, Rogemond V, Chounlamountri N, Kolattukudy PE, Martinez S, *et al.* (2013): Mapping CRMP3 domains involved in dendrite morphogenesis and voltage-gated calcium channel regulation. *J Cell Sci* 126: 4262–4273.

107. Quach TT, Wang Y, Khanna R, Chounlamountri N, Auvergnon N, Honnorat J, Duchemin A-M (2011): Effect of CRMP3 expression on dystrophic dendrites of hippocampal neurons. *Mol Psychiatry* 16: 689–691.

108. Hou ST, Jiang SX, Aylsworth A, Cooke M, Zhou L (2013): Collapsin response mediator protein 3 deacetylates histone H4 to mediate nuclear condensation and neuronal death. *Sci Rep* 3: 1350.

109. Lavery WJ, Barski A, Wiley S, Schorry EK, Lindsley AW (2020): KMT2C/D COMPASS complex-associated diseases [KCDCOM-ADs]: an emerging class of congenital regulopathies. *Clin Epigenetics* 12: 10.

110. Rittschof CC, Bukhari SA, Sloofman LG, Troy JM, Caetano-Anollés D, Cash-Ahmed A, *et al.* (2014): Neuromolecular responses to social challenge: common mechanisms across mouse, stickleback fish, and honey bee. *Proc Natl Acad Sci U S A* 111: 17929–17934.

111. Wu YE, Pan L, Zuo Y, Li X, Hong W (2017): Detecting Activated Cell Populations Using Single-Cell RNA-Seq. *Neuron* 96: 313-329.e6.